Numerical & Experimental Study of Sloshing of Liquid in a Rectangular Tank

Varun Jadon

(ME12M1029)

A Dissertation Submitted to

Indian Institute of Technology Hyderabad

In Partial Fulfillment of the Requirements for

The Degree of Master of Technology

भारतीय प्रौद्योगिकी संस्थान हैदराबाद
Indian Institute of Technology Hyderabad

Department of Mechanical Engineering

December, 2013

Declaration

I declare that this written submission represents my ideas in my own words, and where others' ideas or words have been included, I have adequately cited and referenced the original sources. I also declare that I have adhered to all principles of academic honesty and integrity and have not misrepresented or fabricated or falsified any idea/data/fact/source in my submission. I understand that any violation of the above will be a cause for disciplinary action by the Institute and can also evoke penal action from the sources that have thus not been properly cited, or from whom proper permission has not been taken when needed.
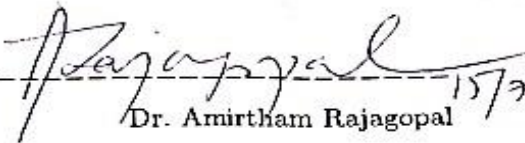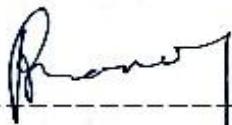
VARUN JADON

ME12M1029

ii

Approval Sheet

This thesis entitled "Numerical & Experimental Study of Sloshing of Liquid in a Rectangular Tank" by Varun Jadon is approved for the degree of Master of Technology from IIT Hyderabad.
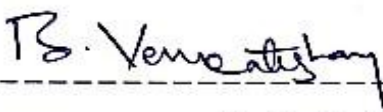
Dr. Amirtham Rajagopal 15/7/14

Assistant Professor,

Department of Civil Engineering,

Indian Institute of Technology, Hyderabad

Examiner

Dr. Raja Banerjee

Associate Professor,

Department of Mechanical & Aerospace Engineering,

Indian Institute of Technology, Hyderabad

Adviser

Dr. Venkatesham B

Assistant Professor,

Department of Mechanical & Aerospace Engineering,

Indian Institute of Technology, Hyderabad

Co-Adviser

iii

Acknowledgements

Dedicated to my country

Abstract

Due to advancement in automobile technology, various types of automobile noises have been reduced significantly and hence sloshing noise has become a major irritant for passengers. Past studies have concluded that the slosh noise is directly connected with the pressure fluctuation dp/dt which in turn can be provided by CFD study of flow dynamics of working fluid in the fuel tank. The present work includes experimental and CFD study of flow dynamics of working fluid in a rectangular tank. Experiments have been performed on indigenously developed Impact test setup. Experiments were conducted with varying fill level, varying sensor location and varying deceleration and the axial acceleration from experiment has been taken as input for CFD analysis. Commercial CFD solver STAR CCM+ was used to perform the CFD simulations. Image validation and dynamic pressure validation has been done to compare the CFD results with experiments.

Contents

Chapter 1: Introduction

1.1 Sloshing

The term Sloshing refers to the movement of liquid inside an object undergoing motion. Whenever a liquid exhibits a free surface, liquid oscillations or sloshing will be introduced by acceleration/deceleration of the container walls. Sloshing of liquids within closed containers thus represents one of the most fundamental fluid-structure interaction problem and has been the subject of many industrial studies like Liquefied Natural Gas (LNG) carriers and their new design, rockets and airplanes fuel reservoirs and road tankers over the past few decades.

With the recent developments in aerospace technology, the size of vehicles, the amount of propellants and the container dimensions have increased which in turn has made the effect of liquid sloshing upon the stability, control and performance of such vehicles more pronounced and dangerous. Instabilities in flight characteristics can result if fuel slosh frequency becomes close to any of the sub-system frequencies. Another well-known practical application of sloshing theory is given by marine engineering research. The loads produced by the wave motion can cause structural damage and even the loss of the motion stability of ships and the liquid motion on the deck of ships can cause mishaps. Often, such waves have a large amplitude and are referred to as non-linear sloshing problems.

A third application of sloshing phenomenon is found in modern automotive industry. Modern automotive technology has undergone recent development in minimizing noise due to engines, tires and aero-acoustics is. Now, the noise

generated due to sloshing fuel within automotive fuel tanks remains as a source of irritation for passengers especially in case of expensive vehicles and hence it has become a subject of debate among all major automotive manufacturers. Sloshing is generated by fluid motions in tank that causes dynamic loads acting on wall and hence noise generation due to vibration of walls on application of these dynamic loads. Passengers perceive sloshing noise as airborne noise and structure borne noise. In airborne noise the sound waves are carried by atmosphere from sound source towards receiver and this type of noise use air, holes across the structure surface as medium of propagation. In structure borne noise sound source acts as source of vibration and these vibrations propagates through car structure to walls of passenger compartment resulting in noise.

Wachowski et al[1] defined the noise generated during sloshing in tank as composed of three different noises which are Hit noise, Splash noise and Clonk noise. These three are differentiated on the basis of their range of frequency.
Splash Noise: Splash Noise is generated due to collision of fluid waves with each other. The principle is shown in Figure 1.1. Its frequency ranges from 0.5-10KHz.
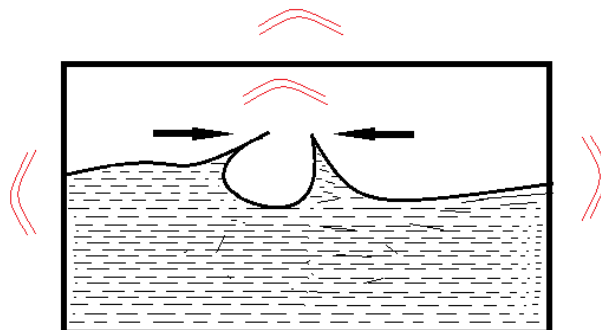
Figure 1.1: Splash Noise

Hit Noise: Hit Noise is generated by wave fronts hitting the walls. Its frequency is in the range of 0.2 to 2 KHz. Sound Intensity of Hit Noise is high because of large mechanical interaction of fluid with the wall and the transmission of hit noise depends on acoustic properties of wall.
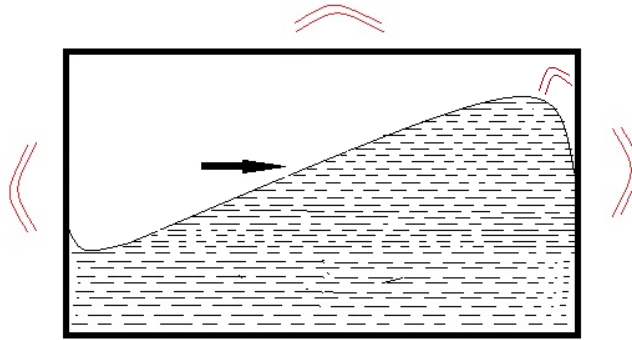
Figure 1.2: Hit Noise

Clonk Noise: This type of noise is generated when abrupt compression of air by sloshing liquid takes place. Its intensity as well as application time is lowest among the three and it occurs in the frequency range of 150-500 Hz.
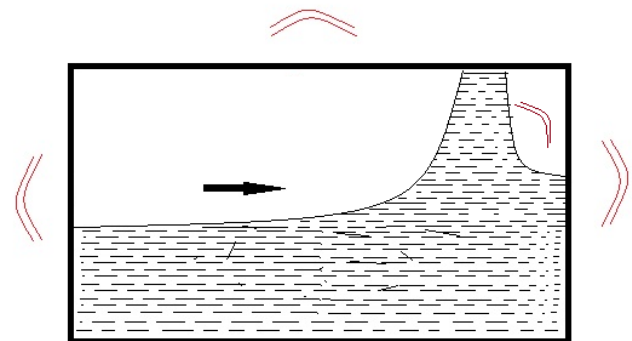
Figure 1.3: Clonk Noise

1.2 Literature Review:

Sloshing due to its applications in a number of industrial areas has been a vast field of research for many decades. The traditional approaches that have been used to assess sloshing loads include linear and nonlinear potential flow theory,

direct experimentation on scaled models and more recently the use of Computational Fluid Dynamics (CFD). Potential flow theory has some limitations and cannot model fluid fragmentation or merging. CFD is thus increasingly being considered as a viable tool for the study of such flows. Early studies of sloshing were confined to jet propelled vehicles only but later this phenomenon became important in many other fields. Khezzar et al.[2]studied sloshing in rectangular tank subjected to impulsive force and concluded that flow visualization of experimental and numerical simulation were similar. Rezaei et al. [3]developed a numerical code for sloshing and validated their results from experiments performed by Hinatsu et al.[4]. The above two studies have concluded that flow dynamics can be efficiently captured in numerical simulation and is comparable to flow visualization recorded during experiments. Wiesche [5] concluded that the sloshing motion and the pressure impulse can be predicted by computational fluid dynamics. The periodicity of sound intensity generation due to sloshing fuel correlates with the fundamental slosh frequency. Furthermore, a correlation between the sound intensity I due to sloshing and the pressure fluctuation dp/dt have been found. Jaiswal et al [6] have conducted experimental and numerical studies on sloshing and have obtained the sloshing frequency of liquid contained in tanks of other shapes and tanks with internal obstructions using Electro-Magnetic Shake Table and ANSYS software. Peric and Zorn [7] studied structural impact of sloshing loads caused by arbitrary motion of tank. The numerical simulation shows good agreement with experimental results. It is also found that there is negligible difference between in results from laminar and turbulent simulations. Thiagrajan et al.[8]worked on sloshing in a rectangular tank using sway excitation and observed that 20% and 80% causes higher pressure than other

4

conditions. Hou et al.[9] applied multiple excitations on a rectangular tank and concluded that liquid sloshing become violent and intensified if sloshing tank is under multiple coupled excitations. Hattori et al [10] studied different types of waves generated due to sloshing and classified them on the basis of impact pressure pattern achieved during experimentation with a specific type of wave. Lugni et al [11]studied the event of "flip through" that takes place during impact of wave on a vertical wall and its effect on dynamic pressure at the wall. Di Matteo et al [12] performed CFD and experimental studies to determine liquid sloshing characteristics during a prescribed sequence of oscillations.

Wasfy et al [13] used time-accurate finite element code that solves turbulent Navier -Stokes equation along with a series of equations that solves multi-body dynamics.

In order to compute sloshing noise from experiments and simulation, Park et al [14] used a Fluid Structure Interaction (FSI) approach to predict noise due to sloshing. Vytla and Ando et al [15] performed a one-way coupled FSI to study the effect of deceleration magnitude for different fuel tank fill level.

1.3: Objective:

The research work documented here is a part of a project dedicated for development of a methodology to predict sloshing noise numerically by giving certain inputs like tank geometry and transient force acting on fuel tank. This work includes CFD study of flow dynamics of working fluid inside the tank. The output of this study i.e. dynamic pressure will be the input for structural and acoustic study to predict sloshing noise.

The first part of this work includes description of experimental setup and procedure used in experimentation study of this work.

The second part includes numerical procedure used for analysis. It includes formulation of numerical models and focuses on interface tracking method used.

The third part is dedicated to results analysis which includes efficacy of numerical procedure using grid independence study, time step independence study and effect of initial surface on after effects of sloshing, Impact test setup experimental results that include inertial acceleration, dynamic pressure and image correlation to some important events. Image validation as well as dynamic pressure validation has been done between CFD and experiments for various cases.

1.4 Outline:

Chapter 1 describes sloshing phenomenon, its applications and sloshing noise. Types of sloshing noise have been discussed.

Chapter 2 deals with experimental procedure and description of experimental setup.

Chapter 3 deals with description of numerical model used. Schemes and mesh type used for numerical solution has been explained.

Chapters 4 deals with results and discussion. It includes mesh independence and time step independence study of numerical model and validation of results.

Chapter 5 discusses about scope of future work in this problem.

Chapter 2: Experimental Test Setup

2.1 Overview:

Experimentation to study sloshing phenomenon can be performed in two ways. One way is to study reciprocating motion of liquid in tank as experienced in LNG carrier ships and civil structures. The other way is to study the sloshing phenomenon due to sudden braking which usually occur in automobiles. An experimental setup to study sloshing phenomenon under control braking load is developed. This setup utilizes the free fall of dead weight to provide acceleration to vehicle and then application of sudden brake is done using band brake. This sudden braking force the fluid to move to and fro in the tank thus creating impact on the tank walls. Figure 2.1 shows the schematic diagram of the indigenously developed Sloshing Phenomenon Experimental setup. It simulates the sloshing phenomenon under control braking load to measure dynamic pressure on the tank-fluid interface and dynamic force on outer surface of tank walls.

The system consists of four major subsystems which are

1.   Loading mechanism,

2.   Braking mechanism

3.   Rectangular tank with provision for sensor mounting

4.   Vehicle travel track.
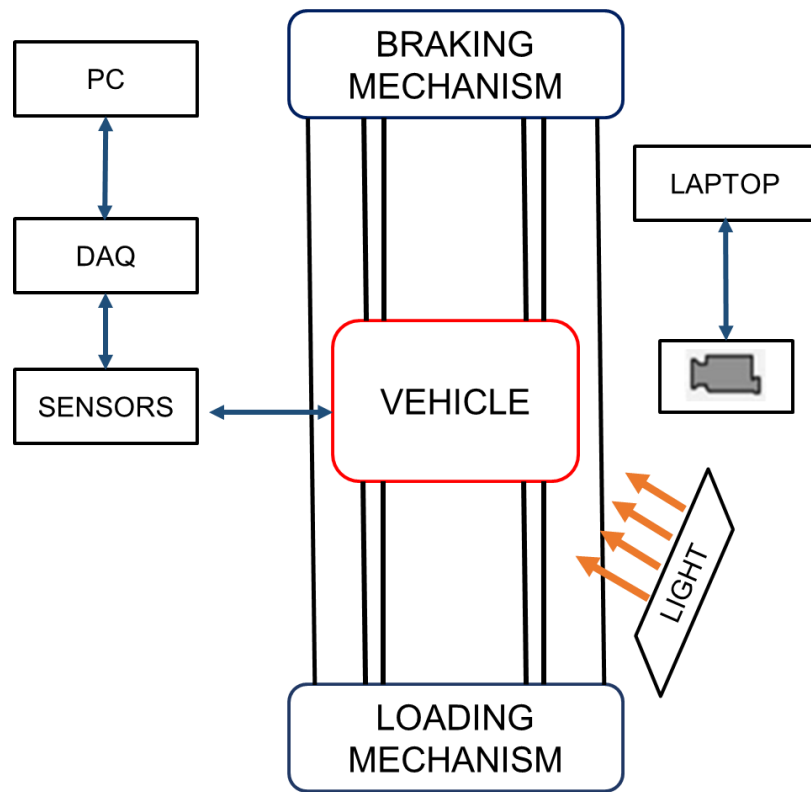
Figure 2.1: Schematic Diagram of Experimental Setup

2.2 Experimental Test Setup:

A transparent rectangular tank made of Acrylic was fabricated with a length of 238 mm, width of 220 mm and height of 238 mm. The tank wall was 6 mm thick. This tank was placed over a wooden platform that was attached to low noise generating wheels in order to reduce background noise. The platform was maintained at a horizontal position with respect to the ground with the help of a spirit level. A three axis linear inertia acceleration sensor (3g-ADXL335) and a line triggering sensor were mounted on this platform. The inertia sensor used to monitor the vehicle acceleration and deceleration. An aluminum track of approximately 1.5 m was prepared on which the vehicle would travel. The aluminum tracks were placed on a wooden base. The aluminum tracks were having continuous groove throughout the length for placing vehicle wheels and this arrangement was done to minimize lateral

8

movement of the vehicle. A string and pulley mechanism is used to attach the vehicle to the dead weight and the free fall of this dead weight under gravity is used to accelerate the vehicle. A band brake is used to apply the brake. Various sensors are mounted on the vehicle to record the effect of this sloshing activity. Dynamic Pressure sensor (Dytran 2300V3) were mounted in the specially prepared slots on tank walls as shown in Figure 2.2. Dynamic Force Sensor (Dytran 1053V3) were mounted on the outer surface of tank walls in front and back direction. The specifications of all the sensors are provided in Table 2.1. These sensors were attached to record the wall vibrations due to impact of fluid on tank walls. Depending on the experimental condition, the sensors can be mounted at 10%, 30%, 50% and 70% of tank height on front and rear wall and at 10%, 50% and 90% on left and right wall Phantom V12.1 high speed camera was used to capture the liquid sloshing behavior. Data from Dynamic Pressure sensors was acquired using HBM DAQ while data from all other sensors were acquired using a NI cDAQ-9178 data acquisition system. A correlation was achieved in between the two DAQ's using force sensors as two force sensors were mounted on the front wall of the acrylic tank, one of which was connected to HBM DAQ while other was connected to the NI DAQ. The whole experimental setup has been shown in Figure 2.3.

Table 2.1: Sensors specification

S. No.	Sensor Name	Range	Sensitivity	Uncertainty
1.	Inertial Accelerometer	±3.6g	300mv/g	±0.0112g
2.	Dynamic Pressure Sensor	500psi	10mv/psi	±0.05855psi
3.	Dynamic Force Sensor	±100lbf	50mv/lbf	±0.01605lbf

High Speed camera Specifications:

Uncertainty in length =0.506 mm

Uncertainty in velocity =5.06e-04 mm/s
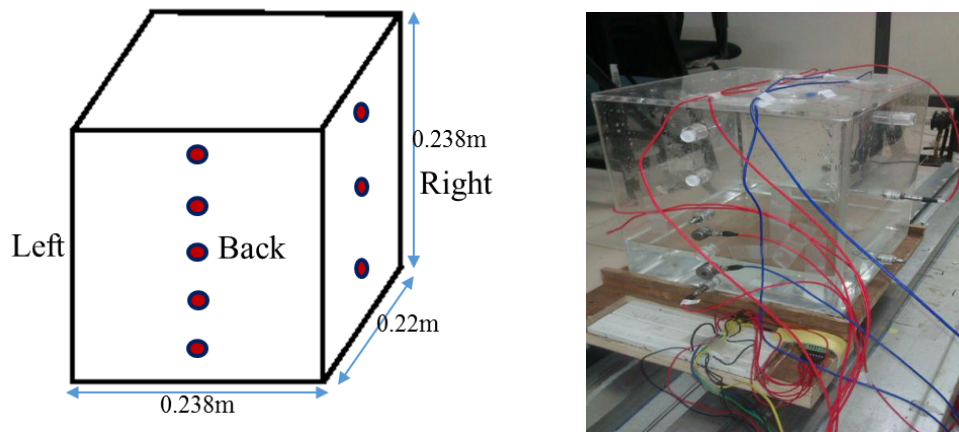
Figure 2.2: Transparent Tank and position of Dynamic Pressure sensors.
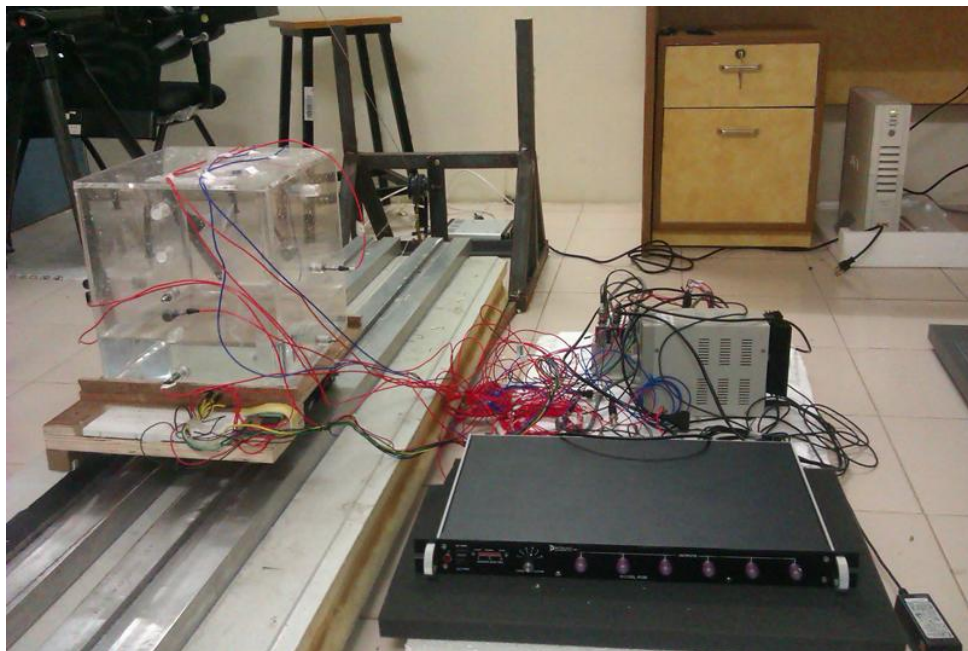
Figure 2.3: Experimental setup

2.3 Experimental Procedure:

Free fall of dead weight accelerates the vehicle on the aluminum track. The vehicle covers a distance of 0.9m before brake application. At a distance of 0.65m from the initial position of vehicle, the line triggering sensor triggers all the sensors as well as high speed camera by changing its output from 0.765 V to 3.5 V. The change in voltage output takes place as the sensor recognizes the change in Infra-red reflectivity of light (from Black to White) from the

track below it. A customized Labview program was used to acquire the data from all the sensors, which was also triggered by the line sensor

The application of sudden brake takes place at the distance of 0.9m from initial position of the vehicle. The acceleration achieved due to free fall of dead weight and deceleration due to sudden braking are estimated from the equations (1) and (2) given below:

$$a=\frac{m_2g-\mu m_1g}{m_1+m_2} \tag{1}$$

$$d=\left(\frac{t_1}{t_2}\right)\left(\frac{m_2g-\mu m_1g}{m_1+m_2}\right) \tag{2}$$

where, m_1 is the mass of the tank with water, m_2 is the mass of the dead weight, a is the acceleration of the tank, d is the deceleration of the tank, t_1 is total time travelled before application of brake, t_2 is required time for deceleration, and μ is coefficient of friction.

This sudden braking generates the sloshing phenomenon inside the tank. Dynamic pressure sensor that are in direct contact with the fluid senses the activity taking place inside the tank and high speed camera captures the flow visualization inside the tank. Various camera settings were used to acquire the video and the present work reports the images that were obtained with a camera frame rate of 1000 fps. An extensive study was conducted to determine repeatability of the test data. Parametric studies were conducted with varying fill levels and sensor locations. Depending on the fill level the position of Dynamic pressure sensors was adjusted. They were kept at 10% of tank height and at 10% of tank height below the fill level in the tank. Table 2.1 provides all the experiments performed in terms of fill level, sensor height and different deceleration value for which the experiments were performed.

11

Table 2.2: Set of experiments performed

S. No.	Fill Level	Deceleration(in g)	Sensors Height
1	20 %	0.20, 0.25, 0.3	10 %
2	40 %	0.20, 0.25, 0.3	10 %, 30 %
3	60 %	0.20, 0.25, 0.3	10 %, 50 %
4	80 %	0.25	10%, 70 %

The major events that were recorded in inertial acceleration sensor and dynamic pressure sensors were analyzed using high speed camera images of that instant. Experimental results have been discussed thoroughly in chapter 4.

Chapter 3: Numerical Model Formulation

3.1 Overview

Sloshing is a complex fluid phenomenon which includes governing equations that cannot be solved analytically. In order to reduce sloshing noise certain modifications need to be made in the tank and then the modified tank need to be simulated experimentally to check the effectiveness of these modifications. This modification is an iterative process and experimenting to check the effectiveness of each incorporated modification is an expensive job in terms of money, time and labor. This necessitates the use of numerical model. Sloshing is a multi-physics phenomenon where fluid mechanics due to liquid sloshing affects structural behavior of the fuel tank and its mountings which in turn affects noise generation and propagation. Thus CFD study of fluid low during sloshing is the first step in this procedure.

The time accurate multiphase CFD modelling was used to capture the sloshing phenomenon when the tank was subjected to a transient axial acceleration and deceleration. The numerical method used in the present work is a finite volume method that solves the integral form governing equations. In this method the governing differential equations are integrated over a control volume enclosed by a control surface. Commercial CFD software Star CCM+ v7.4 [15] was used in this study. Figure 3.1 shows the CFD simulation procedure.

3.2 Computational Grid:

A mesh or grid is defined as a set of point distributed over the problem domain. The process of obtaining an appropriate mesh is termed mesh generation and has long been considered a hindrance in the analysis process due to the lack of a fully automatic mesh generation procedure.
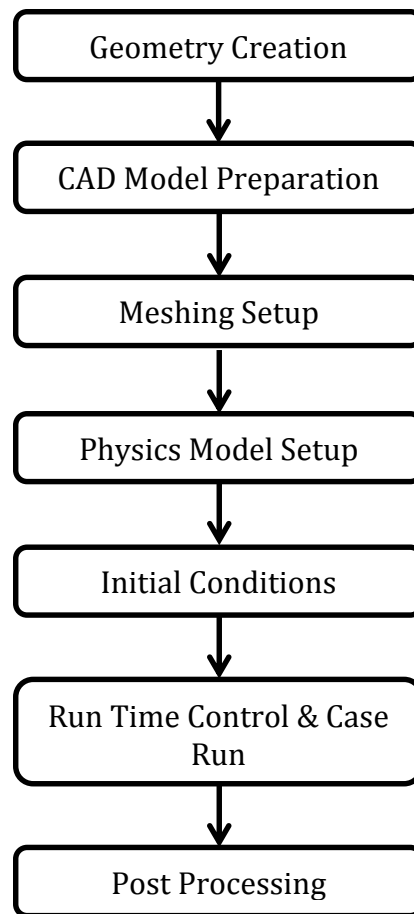
.

```
┌─────────────────────────┐
│   Geometry Creation     │
└─────────────────────────┘
            │
            ▼
┌─────────────────────────┐
│  CAD Model Preparation  │
└─────────────────────────┘
            │
            ▼
┌─────────────────────────┐
│     Meshing Setup       │
└─────────────────────────┘
            │
            ▼
┌─────────────────────────┐
│   Physics Model Setup   │
└─────────────────────────┘
            │
            ▼
┌─────────────────────────┐
│   Initial Conditions    │
└─────────────────────────┘
            │
            ▼
┌─────────────────────────┐
│  Run Time Control & Case│
│           Run           │
└─────────────────────────┘
            │
            ▼
┌─────────────────────────┐
│     Post Processing     │
└─────────────────────────┘
```

Figure 3.1: CFD Simulation Procedure

The elements in a mesh can be classified on the basis of dimension and type of the elements. Common elements in 2D are triangles or quadrilaterals, and common elements in 3D are prisms or polygons.

Mesh can be classified on the basis of connectivity of material.

  i. Structured Meshes

A structured mesh is characterized by regular connectivity that can be expressed as a two or three dimensional array. This restricts the element choices to quadrilaterals in 2D or hexahedra in 3D.

14

ii. Unstructured Meshes

An unstructured mesh is characterized by irregular connectivity is not readily expressed as a two or three dimensional array in computer memory. This allows for any possible element that a solver might be able to use. Compared to structured meshes, the storage requirements for an unstructured mesh can be substantially larger since the neighborhood connectivity must be explicitly stored.

iii. Hybrid Mesh

A hybrid mesh is a mesh that contains structured portions and unstructured portions. The term "mixed" is usually applied to meshes that contain elements associated with structured meshes and elements associated with unstructured meshes (presumably stored in an unstructured fashion).

A three-dimensional geometry of tank is created having the same dimensions as that of tank used in experiment. The meshing options available with Star CCM+ are:

Surface Mesh:

i. Surface remesher

ii. Surface wrapper

Volume Mesh:

i. Advancing layer mesher

ii. Polyhedral mesher

iii. Tetrahedral mesher

iv. Thin mesher

v. Trimmer

Among these following models were used in meshing of this geometry are:

i. Prism layer Mesher

ii. Surface Remesher

iii. Trimmer

Prism layer Mesher is used with a core volume mesh to generate orthogonal prismatic cells next to wall surface or boundaries which makes the solution more accurate near the wall surface. A prism layer is defined in terms of its thickness, the number of cell layers within it, the size distribution and function of distribution for these layers.

Surface Remesher is used to retriangulate the existing surface and hence optimize it for the volume mesh models. The remeshing is based on a target edge length and can refine the mesh based on curvature and surface proximity. It improves the sub surface meshing when prism layer meshing is used.

Trimmer mesh is used for producing high quality grids with minimal cell skewness and the refinement done is based upon the surface mesh size and other control factors. The trimmer meshing model utilizes a template mesh that is constructed from hexahedral cells from which it cuts or trims the core mesh using the starting input surface.

Following are the user defined controls that were taken under consideration while meshing the considered geometry:

i. Base Size:

The base size is a reference length used in other meshing parameters. It can be set either as a relative value or as an absolute value. Mesh independence study was done and base Size=3.671875 mm is taken for geometry under consideration.

ii. Maximum Cell Size:

The maximum cell size limits the largest cell size so that mesh is not too coarse in the center of the domain. It can be set either as a relative value or as an absolute value. It was defined relative to the base size and the value was kept as 100%.

iii. Prism Layer Thickness:

It specifies the total thickness of the prismatic cell layers. It can be set either as a relative value or as an absolute value. It was defined relative to the base size and the value was kept as 10%.

iv. Surface Size:

Surface Size is adopted as minimum and maximum and the size is taken as 100% relative to the base size, both for minimum and maximum.

Impact waves generated after brake application have highly localized profiles and impact pressure acts for very short duration, so accurate calculation of impact pressure requires a fine mesh and corresponding same time step. Since the pressure probe locations are on the extreme edges, so the mesh was made fine on the extreme edges and on the base of the tank.

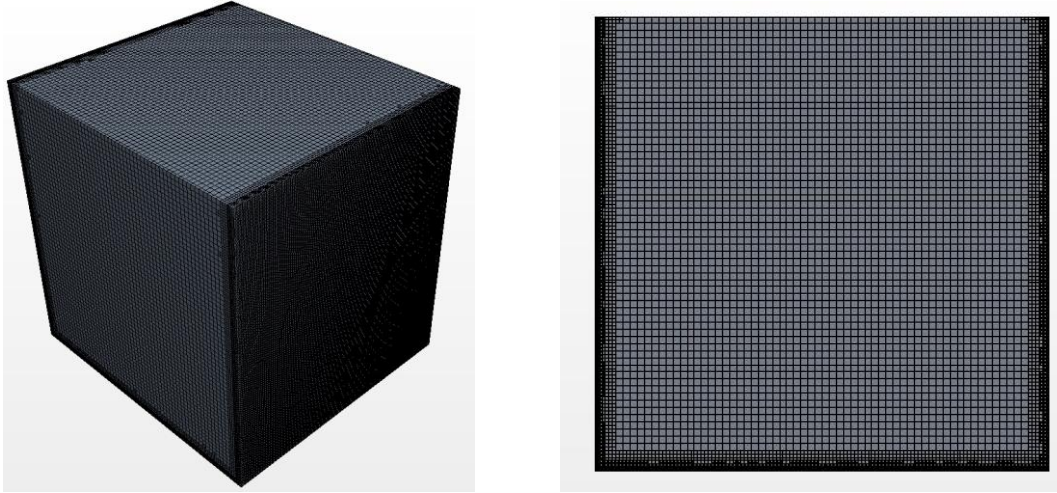Figure 3.2 shows Computational Grid used in 3D and 2D analysis.

Figure 3.2: 3D & 2D Computational Grid

3.3 Numerical Approach:

The Navier Stokes equations are solved by using Segregated or uncoupled Flow algorithm. The linkage between the momentum and continuity equations is achieved with a predictor corrector approach. The method used to solve these equation is based on collocated variable arrangement and Pressure velocity coupling is taken care by Rhie-Chow Interpolation combined with a SIMPLE-type Algorithm[16].

The whole flow field is initialized by some velocity and pressure field thus calculating initial mass fluxes. The flow equations are solved providing an intermediate velocity field and mass fluxes at faces. This intermediate velocity field and fluxes are utilized to solve pressure correction equation and hence giving pressure field as output. The flow equations are again solved using this updated pressure field along with intermediate velocity field. This loop continued till we get a converged pressure field corresponding to predicted velocity field. When both momentum equation and pressure field are converged the solution migrates to next time step.

Equations involved are

Momentum Equation:

$$\frac{\partial}{\partial t}\int_V (\rho v dV) + \int_S \rho v.\mathrm{dS} = -\int_S pI.\mathrm{dS} + \int_S T.dS + \int_V \rho b dV \qquad (3)$$

Continuity Equation:

$$\frac{d}{dt}\int_V \rho dV + \int_S \rho v.dS = 0 \qquad (4)$$

Where ρ stands for fluid density, v stands for fluid velocity vector. Control volume surface under consideration is defined by area S and volume V, T stands for stress tensor, p is the pressure term and I is the kronecker delta function, and b is the body forces vector per unit mass.

Due to high Reynolds number the flow is turbulent. Comparison is done in chapter 4 between different turbulent models and k-ε turbulence model is chosen for further analysis. The Realizable two layer k-ε model is used for turbulence modelling. The k-ε turbulence model is a two –equation model in which transport equations are solved for turbulent kinetic energy k and its dissipation rate ε. Realizable k-ε uses a modified equation for turbulent dissipation rate ε. A critical coefficient of the model Cμ is expressed as a function of mean flow and turbulence properties. This variable Cμ is consistent with experimental observations in boundary layer.   This model combines the Realizable k-ε model with the two layer approach.

The two layer approach allows the k-ε model to be applied in viscous sub-layer. In this approach, the computation is divided into two layers. In the layer next to the wall, the turbulent dissipation rate ε and the turbulent viscosity μ_t, are specified as functions of wall distance. The value of ε specified in the near-wall layer are blended smoothly with the values computed from solving the transport equations far from the wall.

General equation used for modelling k and ε:

$$\frac{d}{dt}\int_V(\rho\Phi dV)+\int_S(\rho\Phi(v-v_g)).dS=\int_S\Gamma\nabla\Phi.dS+\int_V\rho b_\Phi dV \qquad (5)$$

Where ρ stands for fluid density, v stands for fluid velocity vector.

Control volume surface under consideration is defined by area S and volume V, T stands for stress tensor, p is the pressure p and I is the kronecker delta function, Φ defines scalar variable (k or ε), Γ denotes the diffusivity coefficient, b is the body forces vector per unit mass and bφ represents sources or sinks of φ [17] .

The Volume of fluid method is utilized for tracking and locating the free surface motion during sloshing in tank. The VOF method adopts volume fraction as the variable for spatial distribution of each phase at a given time instant. Volume Fraction of a phase can be defined in terms of the ratio of the volume occupied by the phase to the computational cell volume.

The VOF model assumes that velocity, pressure, and temperature fields are shared by all immiscible fluid phases present in a control volume The equations describing mass, momentum ad energy transport are solved in the same way as solved for single phase flow but for an equivalent fluid whose physical properties are calculated as functions of the physical properties of its constituent phase and their respective volume fractions at that time instant[16].

$$\rho=\sum_i\rho_i\alpha_i \qquad (6)$$

$$\mu=\sum_i\mu_i\alpha_i \qquad (7)$$

Where $\alpha_i=\dfrac{V_i}{V}$ is the volume fraction and ρ_i and μ_i are the density and molecular viscosity of the ith phase. The sum value of volume of fraction is one at any point in the flow domain.

$\sum\limits_{i=1}^{n}\alpha_i = 1$, Where n is number of phases present in the flow domain.

The interface is tracked by solving a transport equation for the volume fraction of phases.

For the ith phase, it is expressed as:

$$\frac{d}{dt}\int_V \alpha_i dV + \int_S \alpha_i v.dS = 0 \tag{8}$$

An immiscible phase mixture of water and air is assumed in Sloshing Phenomenon. Since it is an immiscible phase mixture, hence the fluid components are always separated by a sharp interface. The High-Resolution Interface Capturing (HRIC) scheme is used for tracking sharp interfaces. The scheme is based on utilization of a normalized variable $\{\xi\}$[16].

The normalized variable for center cell is defined as

$$\xi_c = \frac{\alpha_C - \alpha_U}{\alpha_D - \alpha_U} \tag{9}$$

The normalized face value ξ_f is defined as

$$\xi_f = \begin{cases} \xi_c & \text{if} \quad \xi_c < 0 \\ 2\xi_c & \text{if} \quad 0 \leq \xi_c < 0.5 \\ 1 & \text{if} \quad 0.5 \leq \xi_c < 1 \\ \xi_c & \text{if} \quad 1 \leq \xi_c \end{cases} \tag{10}$$

The final correction of ξ_f is based on angle θ between normal to interface n_i and the cell face surface vector $\mathbf{a_f}$ as given by:

$$\xi_f^* = \xi_f(\cos\theta)^{C_\theta} + \xi_c(1 - (\cos\theta)^{C_\theta}) \tag{11}$$

The cell face value α_f is calculated as

$$\alpha_f = \xi_f^* (\alpha_D - \alpha_U) + \alpha_U \tag{12}$$

The solution of Navier-Stokes equations follows the segregated iterative method, in which the linearized momentum component equations are solved first using prevailing pressure and mass fluxes through cell faces (inner

iterations), followed by solving the pressure-correction equation derived from the continuity equation. SIMPLE Algorithm is used to solve the Navier-Stokes equation and converged velocity field is achieved for each time step. After getting corrected velocity field from momentum equation, equations for volume fraction and k-epsilon model are solved. The whole process moves to next time step when residual of all the equations included in this process is reduced to a defined level.

Boundary Condition for all the faces of tank is described as no-slip wall. No slip wall means that the tangential velocity is set either to zero or to a specified value. In our test case the value is assigned as zero. The boundary face pressure is extrapolated from the adjacent cell using reconstruction gradients. As the computational domain fully enclosed, a location for reference pressure is defined at center of top wall of tank.

The Simple Algorithm used in numerical study is discussed in flow chart given in Figure 3.3
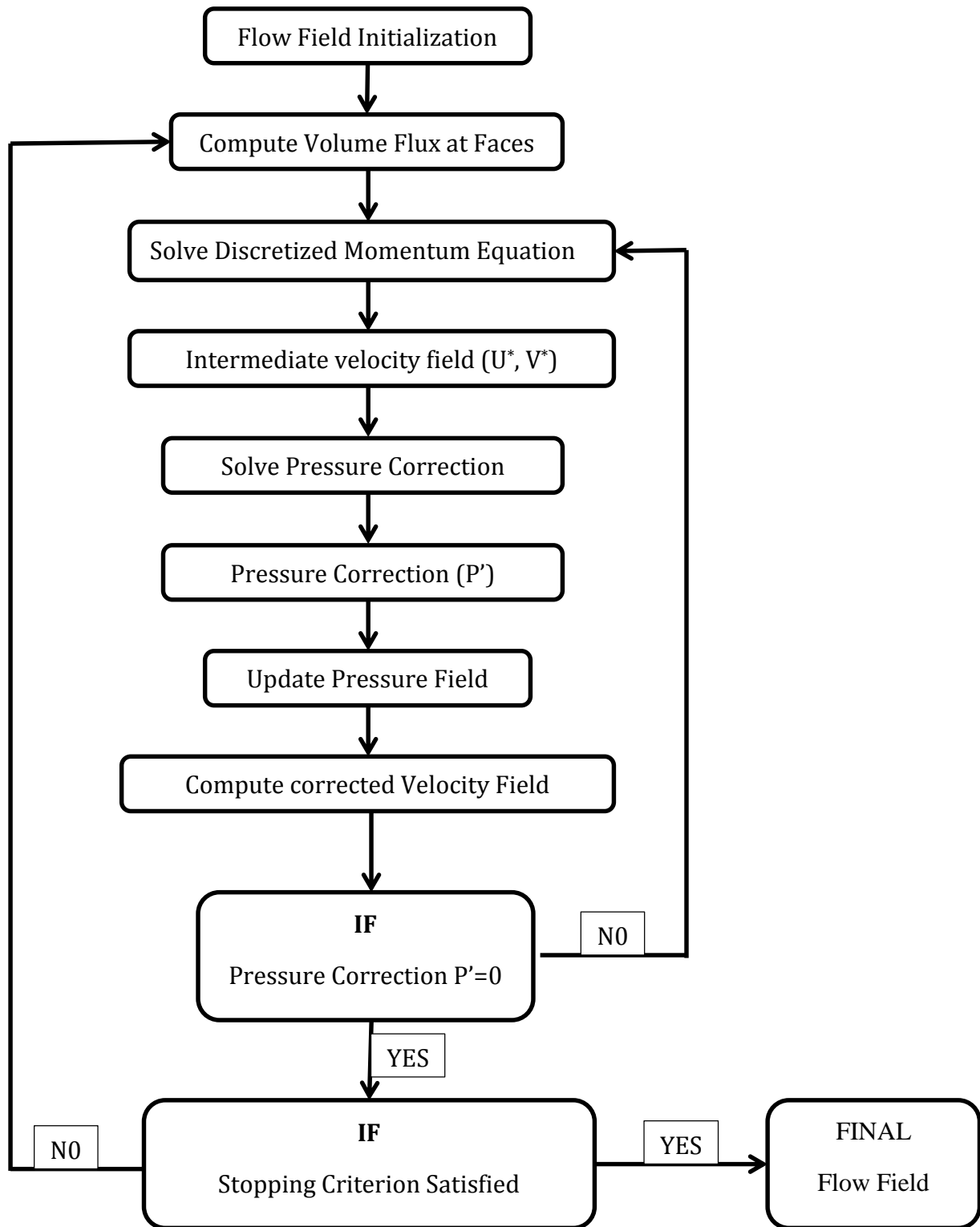
Figure 3.3: SIMPLE Algorithm

The flowchart contains the following boxes and connections:

- Flow Field Initialization
- Compute Volume Flux at Faces
- Solve Discretized Momentum Equation
- Intermediate velocity field (U*, V*)
- Solve Pressure Correction
- Pressure Correction (P')
- Update Pressure Field
- Compute corrected Velocity Field
- IF Pressure Correction P'=0
- IF Stopping Criterion Satisfied
- FINAL Flow Field

Decision labels: N0 (from IF Pressure Correction P'=0 back to Solve Discretized Momentum Equation), YES (from IF Pressure Correction P'=0 to IF Stopping Criterion Satisfied), N0 (from IF Stopping Criterion Satisfied back to Compute Volume Flux at Faces), YES (from IF Stopping Criterion Satisfied to FINAL Flow Field).

Chapter 4: Experimental Results

In this section, the experimental test result data for the various parametric studies are discussed t. During experimentation, the dead weight mass was so adjusted such that a deceleration value of 02g, 0.25g and 0.3g was obtained. The sensors were placed at a height of 10 % of tank height and 10 % below the liquid surface. It is observed from the inertia acceleration sensor data that acceleration in downward direction (Z direction) is 1 g and is constant with time. Lateral acceleration (Y) is less than 0.1 g and therefore indicating negligible lateral movement.

The Figures show the recorded test data of inertia acceleration in longitudinal direction, dynamic force on the front and rear wall of the vehicle motion, dynamic pressure on the inside front, rear and side tank walls. A line sensor placed on the vehicle triggers the data acquisition system as the sensor recognizes the change in Infra-red reflectivity of light (from Black to White) from the track below it. In vehicle moving direction the braking events starts after either 0.49 second or 0.99 second. The braking time depends upon the fill level and dead weight used to impart acceleration to vehicle. The required deceleration is achieved for a duration of 0.5 second. After the braking event, the dynamic sensors start showing observable variation in data and the sloshing phenomenon is recorded by the high speed camera.

Results discussed here are tabulated in such a way that first plot represents the inertial acceleration in longitudinal direction while the second plot represents the dynamic force measured on front and rear walls and the third plot represents the dynamic pressure measurements. Below the plots, high speed camera images are given that corresponds to the major events discussed for that case and these images are provided with the time of the

event they correspond to. The first image corresponds to the condition inside the tank when the brake is applied. Application of brake is taken as the event when the part of fluid has moved towards the front wall. This event is characterized by the peak shown in the front wall pressure sensor. The second image belongs to the event when the back pressure sensor has shown a sudden rise in pressure while the third event belongs to activity at front wall.

The set of experiments performed is already given in Table 2.1. Following points are discussed for analysis for each experiment:

i. Activity inside the tank at some important instances of time.

ii. Effect of deceleration value on different parameters.

iii. Effect of sensor location on different parameters for a constant deceleration.

iv. Transition of sloshing from non-linear to linear regime.

All experiments were performed with the following constant physical conditions:

i. Starting point of vehicle is always fixed.

ii. End point of vehicle is always fixed.

iii. DAQ and camera is triggered at a distance of 0.65m from starting point and application of brake takes place after 0.25 m from trigger point.

4.1 Experimental Data Analysis

Fill level =20%, sensor location =10%, Deceleration=0.2g
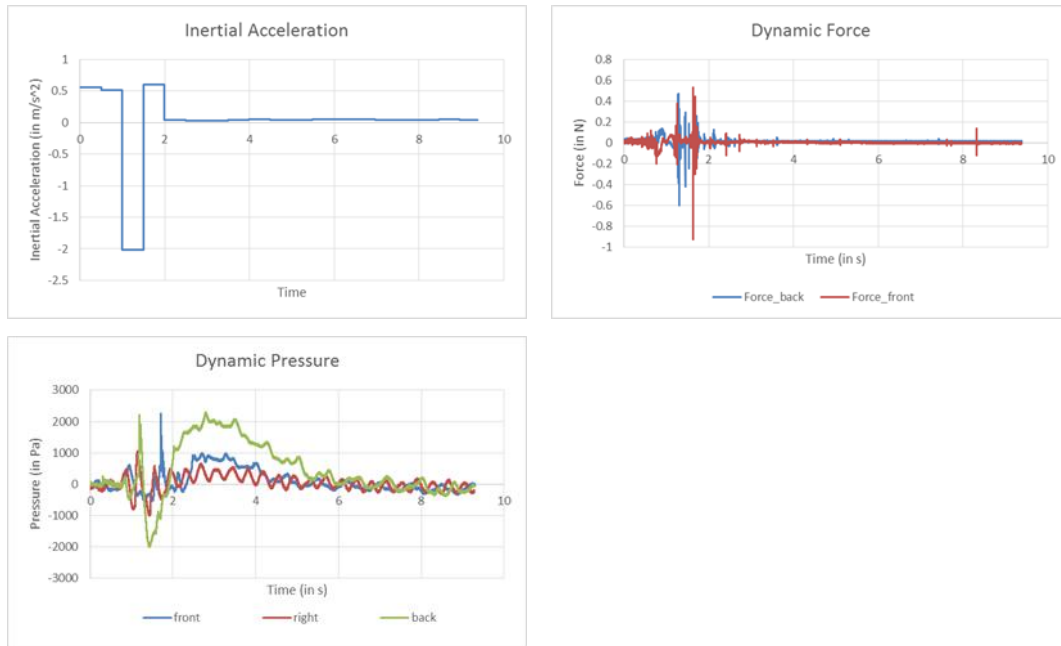
Figure 4.1: Fill level=20%, Sensor=10%, Deceleration=0.2g
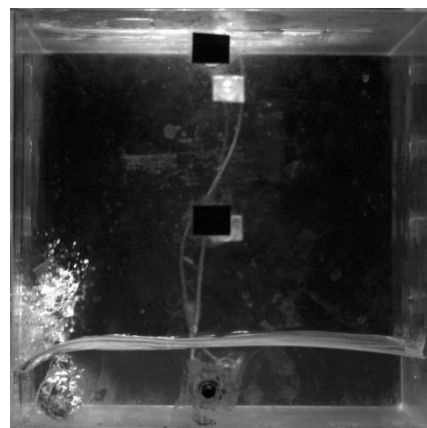
Inertial acceleration graph in Figure 4.1.1 shows that braking starts at 1.0 s and ends at 1.5s.
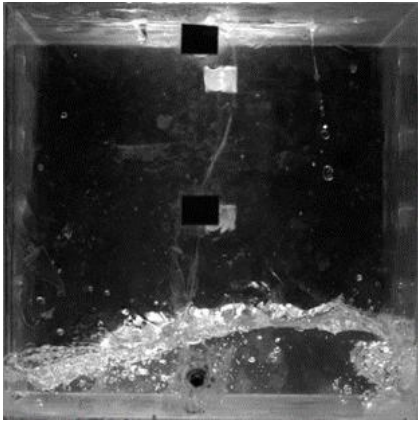
Acceleration jump when braking starts= 2.535m/s^2

Acceleration jump when vehicle stops= 2.623m/s^2
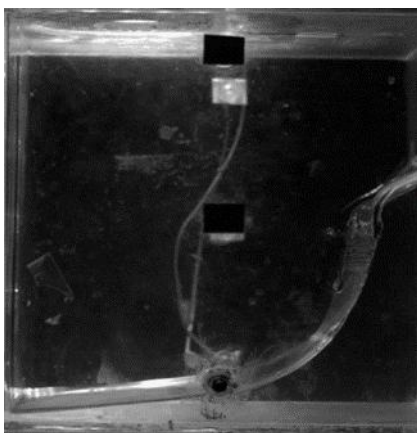
Event-1 (1.0s)

Event-2(1.215s)

Event-3 (1.621s)

Figure 4.2: Image correlation for Fill level=20%, Sensor=10%, Deceleration=0.2g

The condition of fluid inside the tank at the time of brake application (0.99s) when analyzed from high speed camera image revealed that a major part of fluid has already moved towards the front wall. This movement of fluid was sensed by front pressure sensor as it has given a corresponding peak at time of brake application. After brake application the vehicle will move some distance in the opposite direction due to the elasticity of the string used for brake application. This movement of the vehicle as indicated from the inertial acceleration sensor continued for approximately another 0.5s.

Dynamic force and dynamic pressure plots show that the first hit event occurred at the rear wall which is followed by the second event at the front wall. The fluid moves towards the rear wall and makes an impact on the rear wall at 1.20s and this event has been captured by both the dynamic type sensors. This impact at rear wall is recorded as non-linear sloshing event in high speed camera image where the fluid hits the wall violently and a part of this fluid has surged over the rear wall. This upward movement of fluid over the rear wall continued and a part of fluid hits the top surface of the tank.

The event 2 occurs when fluid moves back towards the front wall and this movement is sensed by the sensor attached at the right wall of the tank. The

right pressure sensor shows a peak in between the two events. The right pressure sensor is attached at side wall which is intermediate to front and rear wall and hence the side pressure sensor records an intermediate peak in between the activity at front and rear wall. The fluid hits the front wall and the amplitude of impact has increased which is observed by the difference in magnitudes of the two events as recorded by the dynamic sensors. This increment in amplitude can be due to difference in mass hitting the wall or a synchronous motion of liquid in the rear end of the tank due to the non-linear regime of sloshing. This event is also accompanied by upward movement of fluid along the front wall and then hitting the top surface of the tank.

After two set of events the dynamic force sensors do not show any significant corresponding events although the dynamic pressure still shows some activity taking place inside the tank. The sloshing phenomenon inside the tank is now transitioning towards the linear sloshing regime. This is well supported by high speed camera images. .

Following observations can be made from the plots shown in Figure 4.1

1st impact at rear wall: 1.19s

Dynamic Pressure=2180.51 Pa

Dynamic Force=0.473 N

2nd impact at front wall: 1.707s

Dynamic Pressure=2124 Pa

Dynamic Force=0.53 N

Time difference in between event 1 and event 2 = 0.20s

Time difference in between event 2 and event 3 = 0.51s

Time taken in transition from non-linear to linear sloshing =5s

Fill level =20%, sensor location =10%, Deceleration=0.25g

Inertial acceleration graph in figure 4.3 shows that braking starts at 1.0 s and ends at 1.5s.

Acceleration jump when braking starts= 3.305 m/s^2

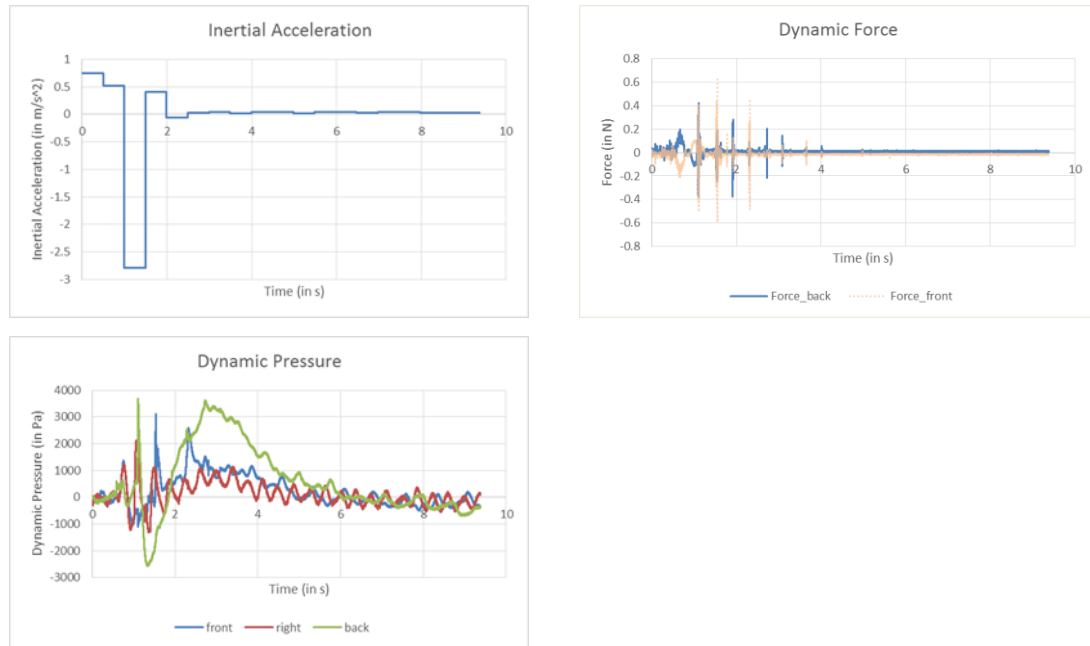Acceleration jump when vehicle stops= 3.186 m/s^2

Figure 4.3: Fill level=20%, Sensor=10%, Deceleration=0.25g

At the time of brake application, most part of the fluid has already moved towards the front wall and this movement is shown by front dynamic pressure sensor at 0.99s. The movement of the vehicle in the opposite direction after brake application continued for approximately 0.5s

Dynamic force and dynamic pressure plots show that the first event occurs at the rear wall which is followed by the second event at the front wall. The fluid moves towards the rear wall and makes an impact on the rear wall at 1.10 s and this event is captured in both the dynamic type sensors. This impact at rear wall is recorded as non-linear sloshing event in high speed camera image where the fluid hits the wall violently and a part of this fluid has climbed upon the rear wall thereby hitting the top surface.

29
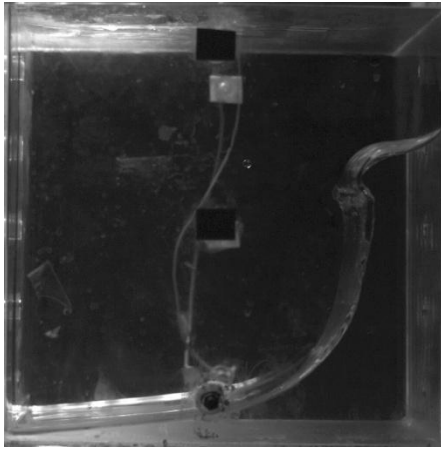
Event 1 (0.99s)
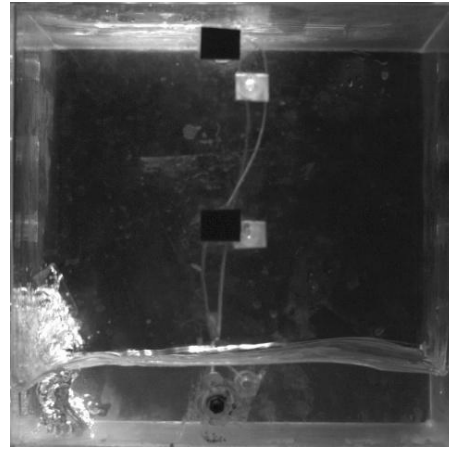
Event 2 (1.0955s)
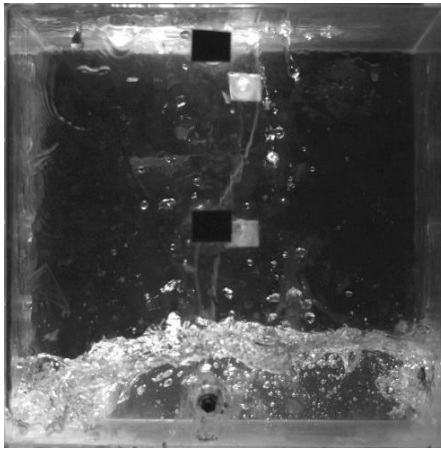
Event 3 (1.523s)

Figure 4.4: Image correlation for Fill level=20%, Sensor=10%, Deceleration=0.25g

Event 3 occurs when the fluid moves back towards the front wall and this movement is sensed by the sensor attached at the right wall of the tank. The fluid hits the front wall although the amplitude of impact is lower as observed by the difference in magnitudes of the two events as recorded by the dynamic sensors at 1.533s. The high speed camera image corresponding to this event shows that a part of fluid is just hitting the front wall thus creating impact on the wall.

Comparison of dynamic force acquired during these two events shows that dynamic force is higher for impact on rear wall as compared to front wall and similar observation is also made in case of dynamic pressure sensor.This

observation may be due to the air entrapped between the liquid and wall as seen in the high speed video images. This decreases the impact loading on the walls.

After the two set of events the dynamic force sensors do not show any corresponding events although the dynamic pressure still shows some activity taking place inside the tank and the flow is transitioning towards the linear slosh regime. This is well supported by high speed camera images.

Following observations can be made from the plots shown in Figure 4.3

1st impact at rear wall: 1.105s

Dynamic Pressure=3686 Pa

Dynamic Force=0.765 N

2nd impact at front wall: 1.533s

Dynamic Pressure=3110 Pa

Dynamic Force=0.583 N

Time difference in between event 1 and event 2 = 0.115s

Time difference in between event 2 and event 3 = 0. 428s

Time taken in transition from non-linear to linear sloshing =5s

Fill level =20%, sensor location =10%, Deceleration=0.3g

Inertial acceleration graph in Figure 4.5 shows that braking starts at 0.5s and ends at 1.0s.

Acceleration jump when braking starts= 3.78 m/s^2

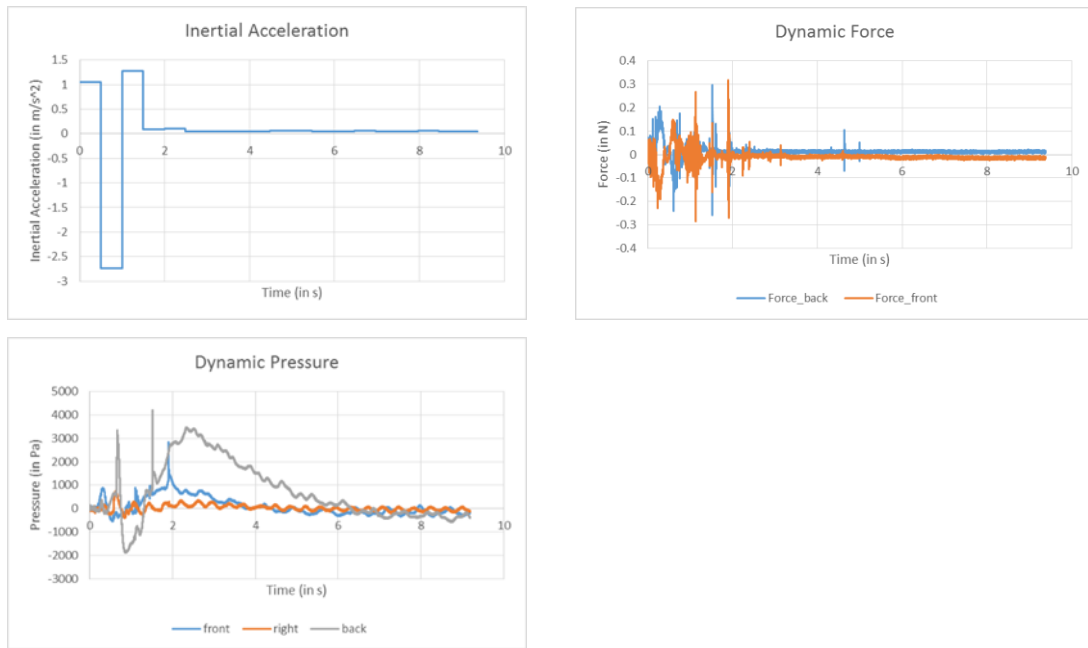Acceleration jump when vehicle stops= 4.00 m/s^2

Figure 4.5: Fill level=20%, Sensor=10%, Deceleration=0.3g

At the time of brake application, most part of fluid has already moved towards the front wall and this movement is shown by dynamic front sensor at 0.49s. The reverse movement of vehicle after brake application continued from 0.49s to 0.99s.
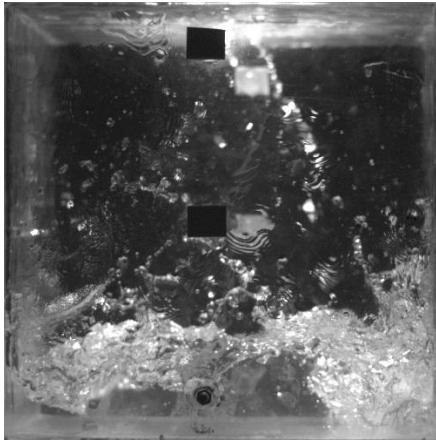
Dynamic force and dynamic pressure plots show that the first event occurs at the rear wall which is followed by the second event at the front wall.
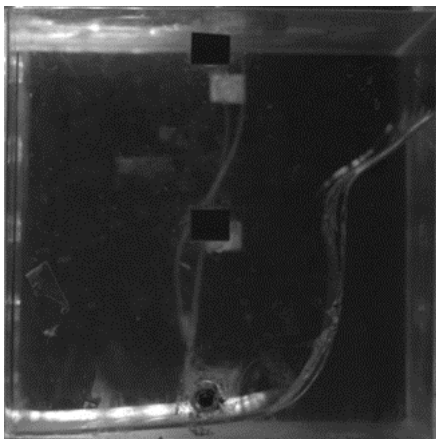
Event 1 (0.49s)
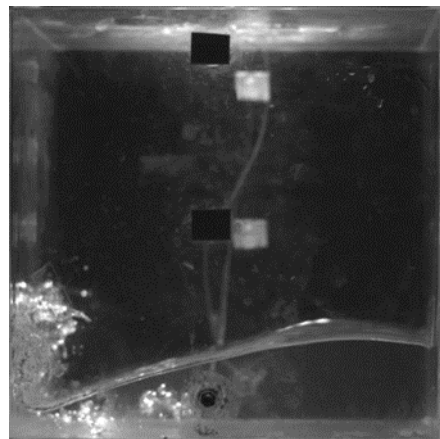
Event 2 (0.65s)

Event 3 (1.12s)

Figure 4.6: Image Correlation: Fill level=20%, Sensor=10%, Deceleration=0.3g

The fluid moves towards the rear wall and makes a large impact on the rear wall at 0.67 s and this event has been captured in both the dynamic quantities sensor. This impact at rear wall is recorded as non-linear sloshing event as seen in high speed camera image. The liquid hits the wall violently and a part of this fluid climb upon the rear wall and hits the top surface of the tank.

Event 3 occurs when the fluid moves back towards the front wall and this movement is determined. The right pressure sensor shows a peak between event 2 and 3. The fluid hits the front wall with a lower amplitude as observed by the data recorded by the dynamic sensors at 1.12s. The high speed camera image corresponding to this event shows that a part of fluid is just hitting the front wall thus creating impact on the wall.

Dynamic force data observed during event 2 and 3 show similar amplitude. However the dynamic pressure at event 3 is significantly smaller than at event 3. This is because there is large liquid sloshing at the end of event 2. The liquid thus climbs the rear wall and falls near the front wall of the tank. The remaining liquid travels forward towards the front wall. This liquid wave interacts with the liquid that is dropping from the roof of the tank. This

33

interaction occurs near the front dynamic pressure sensor and therefore its response gets muted.

Following event 3, the liquid again moves towards the rear wall. This time the dynamic pressure sensor records a much higher response as the impact zone is free of any entrained air bubbles. The liquid completes two sloshing cycles and then the flow transition to linear sloshing regime begins. This is supported by high speed video images and each of any major events that is recorded by dynamic force sensor.

Following observations can be made from the plots shown in Figure 4.5:

1st impact at rear wall: 0.6659 s

Dynamic Pressure=3361 Pa Dynamic Force=0.2 N

2nd impact at front wall: 0.941 s

Dynamic Pressure=890 Pa

Dynamic Force=0.27 N

Time difference in between event 1 and event 2 = 0.165s

Time difference in between event 2 and event 3 = 0. 268s

Time taken in transition from non-linear to linear sloshing =6.5s

Fill level =40%, sensor location =30%, Deceleration=0.2g

Inertial acceleration graph in figure 4.7 shows that braking starts at 1.0 s and ends at 1.5s.

Acceleration jump when braking starts= 2.52m/s^2

Acceleration jump when vehicle stops= 2.15m/s^2

Analysis of high speed camera image at the instant of brake application suggested that a major part of the fluid has already moved towards front wall. This movement is captured by the dynamic pressure sensor located at front

wall. After application of brake the vehicle move in opposite direction and this movement is determined by inertial acceleration sensor for approximately 0.5s.
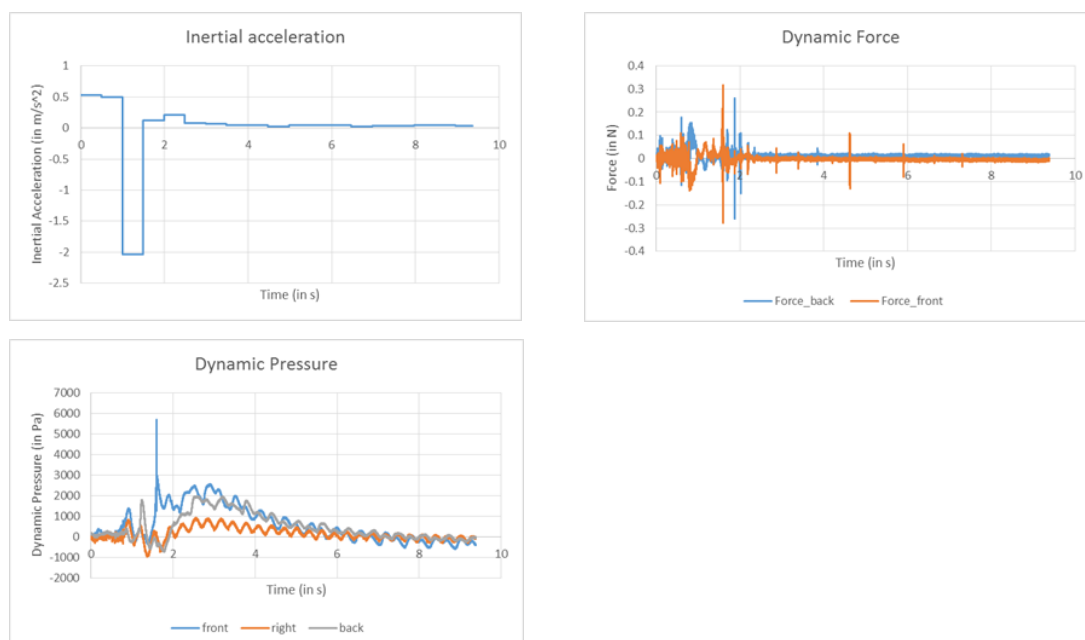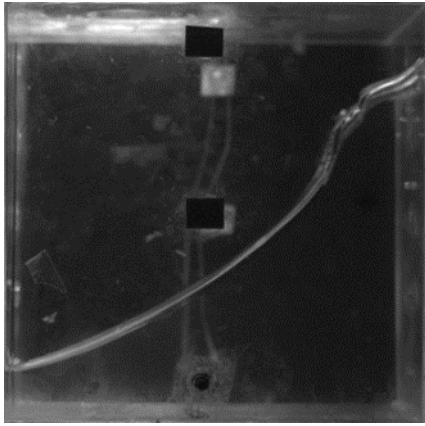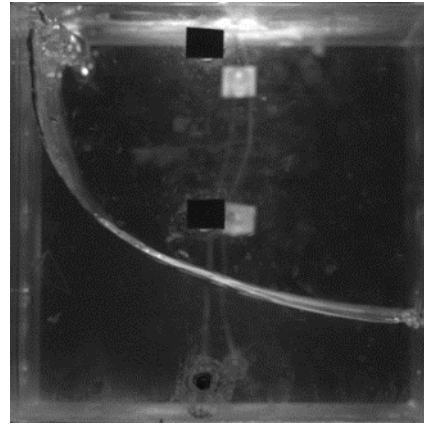

Figure 4.7: Fill level=40%, Sensor=30%, Deceleration=0.2g

Dynamic type sensor data show that the first hit event occurs at the rear wall which is followed by the second event at the front wall. The fluid moves towards the rear wall and smoothly surges over the rear wall and reaching maximum height at 1.238 s and this event has been captured in dynamic pressure sensor only. This event is not recorded in acceleration and force sensor as the process of fluid surging up the wall takes place smoothly and as such there is no direct hit on the wall. The dynamic pressure sensor acquires this event as it is in contact with fluid and hence it can detect dynamic activity of fluid inside the tank.
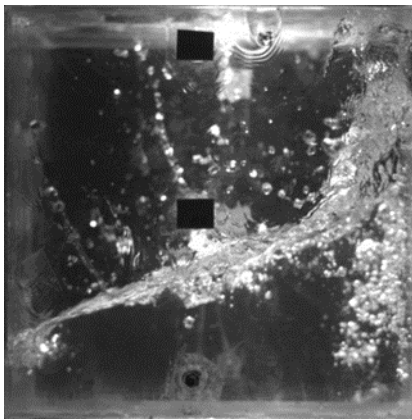
Event 3 occurs when the fluid moves back towards the front wall and this movement is sensed by the side dynamic pressure sensor. The right pressure sensor shows an intermediate peak between events 2 and 3. The fluid hits the front wall and makes an impact on the wall and this event has been captured in both the dynamic type sensors.

Event-1 (0.99s)

Event-2 (1.25s)

Event-3 (1.589s)

Figure 4.8: Image Correlation: Fill level=40%, Sensor=30%, Deceleration=0.2g

The fluid moves back towards the rear wall and this movement of fluid can be differentiated in two regions: one wave-front region which is coming from front wall with large velocity and one region in which large mass is moving upward along the back wall with small velocity. Before the wave front reaches front wall the large mass has already passed the pressure sensor level and the wave front impact takes place at certain height from the pressure sensor. This impact is detected by dynamic force sensor and dynamic pressure sensor. This impact is smaller in magnitude as compared to impact at front wall.

After two set of events, dynamic force sensors do not show any significant events but the dynamic pressure still shows some activity taking place inside the tank. The sloshing phenomenon inside the tank is now transitioning

36

towards the linear sloshing regime which is well supported by high speed camera images.

Following observations can be made from the plots shown in Figure 4.7:

1st impact at rear wall: 1.25s

Dynamic Pressure=1733 Pa

Dynamic Force=0.1 N

2nd impact at front wall: 1.589s

Dynamic Pressure=5688 Pa

Dynamic Force=0.32 N

Time difference in between event 1 and event 2 = 0.25s

Time difference in between event 2 and event 3 = 0.24s

Time taken in transition from non-linear to linear sloshing =5.5s

Fill level =40%, sensor location =10%, Deceleration=0.2g

Inertial acceleration graph shows that braking starts at 1.0s and ends at 1.5s.

Acceleration jump when braking starts= 2.36 m/s^2

Acceleration jump when vehicle stops= 1.84 m/s^2

The condition at the time of braking will remain same as loading has not been changed, only the sensor position has been changed.
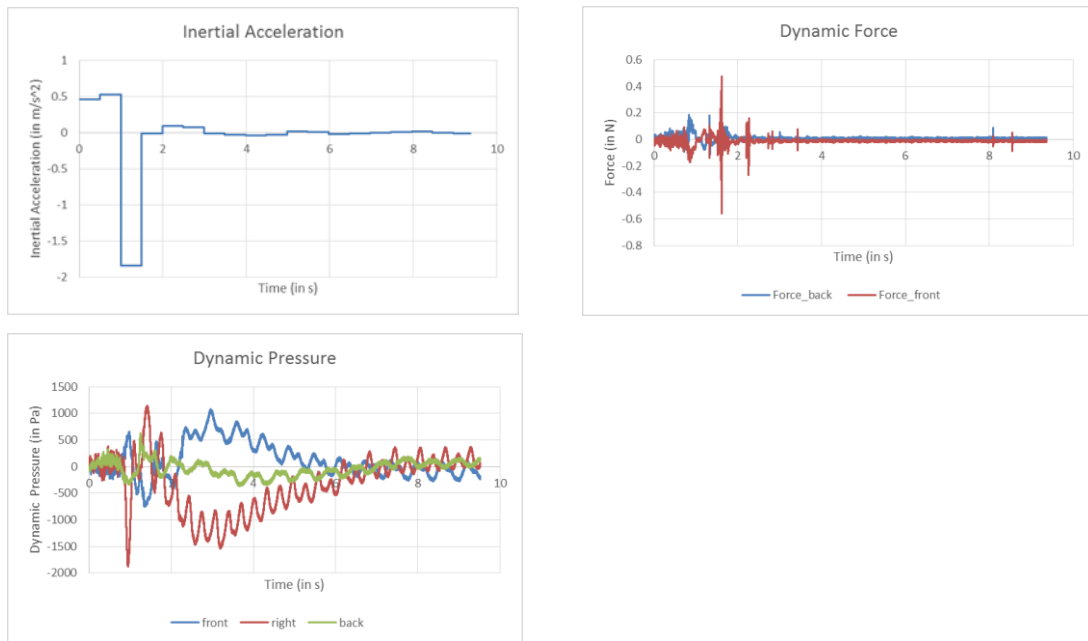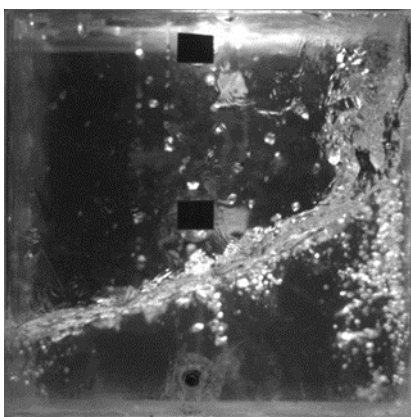
Figure 4.9: Fill level=40%, Sensor=10%, Deceleration=0.2g

Event 1 occurred at same time frame and the event 2 i.e. event corresponding to movement of fluid towards rear wall also occurred at same time as the transition of fluid was smooth and no impact was observed. However since no significant dynamic activities are taking place at the bottom of the tank and the data recorded in dynamic pressure sensor is smaller as compared to sensor at 30 percent of tank height. The dynamic force sensor does not show any significant change at this moment of time as there is no impact on wall.

Event 3 (1.654s)

Figure 4.10: Image Correlation: Fill level=40%, Sensor=10%, Deceleration=0.2g

Event 3 occurred when the fluid moves back towards the front wall and this movement is sensed by the sensor attached at the side wall of the tank as an intermediate peak in between the events 2 and 3. The fluid hits the front wall and this hit is observed by the dynamic force sensor at same time when it was recorded by sensors at 30 percent of tank height but the dynamic pressure sensor records the event at front wall at 1.654s. This is due to the position of this dynamic pressure sensor. The dynamic force sensor will sense the vibration of the wall as a whole but the dynamic pressure sensor at front will sense the activity taking place inside the tank. At 10 percent of tank height there is not much dynamic events taking place and hence it will show the peak value when the fluid has reached up-to maximum height which is the same as observed in high speed camera image at that instant.

After the two set of events the dynamic force sensors do not show any corresponding events although the dynamic pressure still shows some activity taking place inside the tank. The sloshing phenomenon inside the tank is now transitioning towards the linear sloshing regime and is well supported by high speed camera images.

Following observations can be made from the plots shown in Figure 4.9:

1st impact at rear wall: 1.105s

Dynamic Pressure=616 Pa

Dynamic Force=0.765 N

2nd impact at front wall: 1.654s

Dynamic Pressure=480 Pa

Dynamic Force=0.5 N

Time difference in between event 1 and event 2 = 0.115s

Time difference in between event 2 and event 3 = 0. 428s

Time taken in transition from non-linear to linear sloshing =6.5s

Fill level =40%, sensor location =30%, Deceleration=0.25g

Inertial acceleration graph in Figure 4.11 shows that braking starts at 0.5 s and ends at 1.0s.

Acceleration jump when braking starts= 3.56m/s^2

Acceleration jump when vehicle stops= 2.93m/s^2

The condition of fluid inside the tank at the time of brake application (0.49s) when observed from high speed camera image revealed that a major part of fluid has already moved towards the front wall and is sensed by the front dynamic pressure sensor. After brake application the vehicle will move some distance in the opposite direction is recorded by the inertial acceleration sensor continued for approximately 0.5s
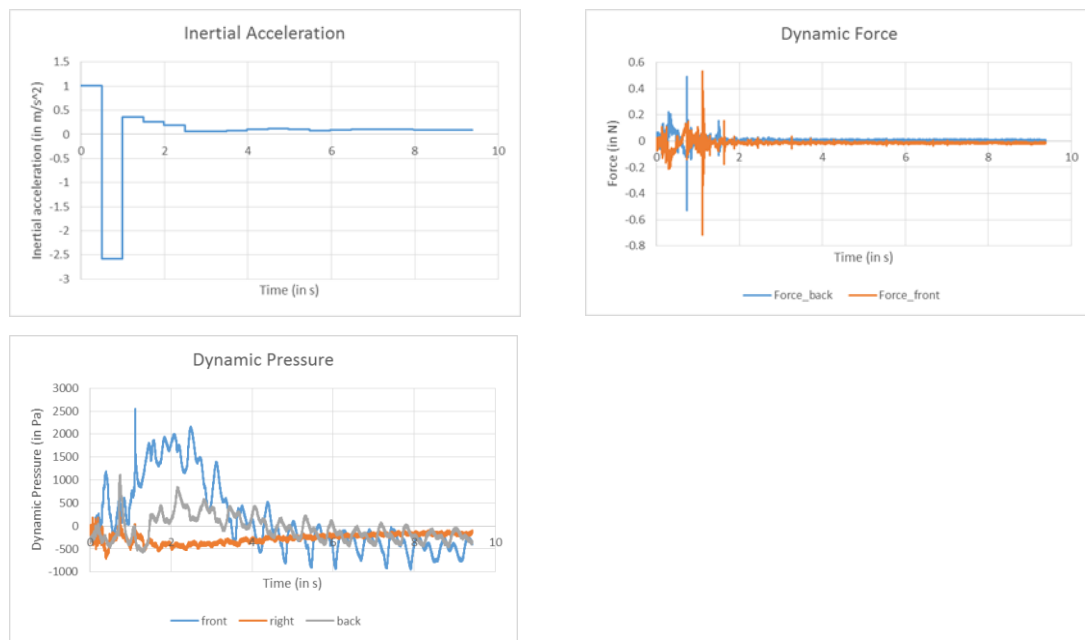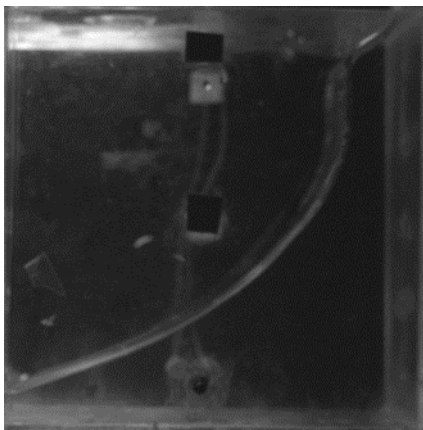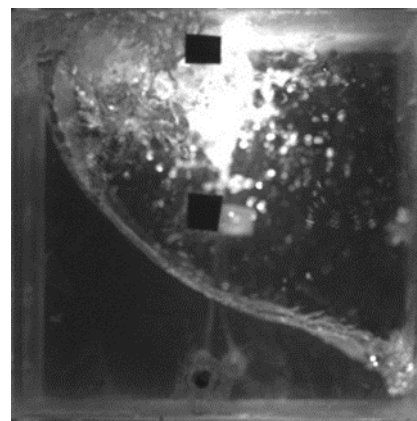

Figure 4.11: Fill level=40%, Sensor=30%, Deceleration=0.25g

Dynamic pressure plots show that the first hit event occurs at the rear wall which is followed by the second event at the front wall. The fluid moves towards the rear wall and smoothly surge over the rear wall and reaching maximum height at 0.738 s and this event is captured in the dynamic pressure sensor only. At this moment of time the fluid has reached to the tank roof and

a part of it hits the top surface and gets deflected back towards the bottom of the tank. This event is not recorded as a significant peak in the force sensor. Event 3 occurred when the fluid moves back towards the front wall. The fluid hits the front wall and makes an impact on the wall and this event has been captured in dynamic type sensors. The force sensor shows the same amount of force as detected during 1st event on rear wall.

Event-1 (0.5 s)

Event-2 (0.74s)
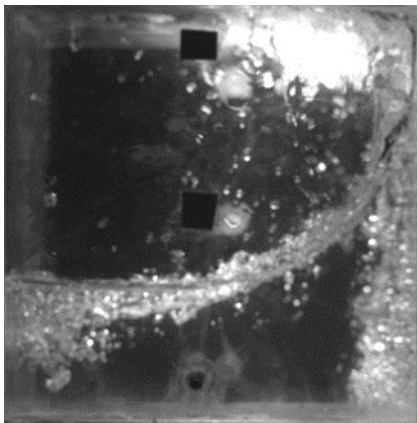
Event-3 (1.113s)

Figure 4.12: Image Correlation: Fill level=40%, Sensor=30%, Deceleration=0.25g

The fluid moves back towards the rear wall and this movement of fluid is very smooth and hence no such comparable peak is shown in pressure sensor. Although the force have recorded some activity which is due to wave front hitting the rear wall of the tank.

After two set of events the dynamic force sensors do not show any significant corresponding events although the dynamic pressure still shows some activity taking place inside the tank. The sloshing phenomenon inside the tank is now transitioning towards the linear sloshing regime. This is well supported by high speed camera images.

Following observations can be made from the plots shown in Figure 4.11:

1st impact at rear wall: 0.74s

Dynamic Pressure=1099 Pa

Dynamic Force=0.48 N

2nd impact at front wall: 1.113s

Dynamic Pressure=2417 Pa

Dynamic Force=0.53 N

Time difference in between event 1 and event 2 = 0.29s

Time difference in between event 2 and event 3 = 0.62s

Time taken in transition from non-linear to linear sloshing =1.5 s or 2cycles

Fill level =40%, sensor location =10%, Deceleration=0.25g

Inertial acceleration graph in Figure 4.13 shows that braking starts at 1.0s and ends at 1.5 s.

Acceleration jump when braking starts= 3.47 m/s^2

Acceleration jump when vehicle stops= 2.78 m/s^2

The condition at the time of braking will remain same as loading has not been changed, only the sensor position has been changed. The event 1 occurred at same time frame and the event 2 i.e. event corresponding to movement of fluid towards rear wall also occurred at same time as the transition of fluid was smooth and no impact was observed.
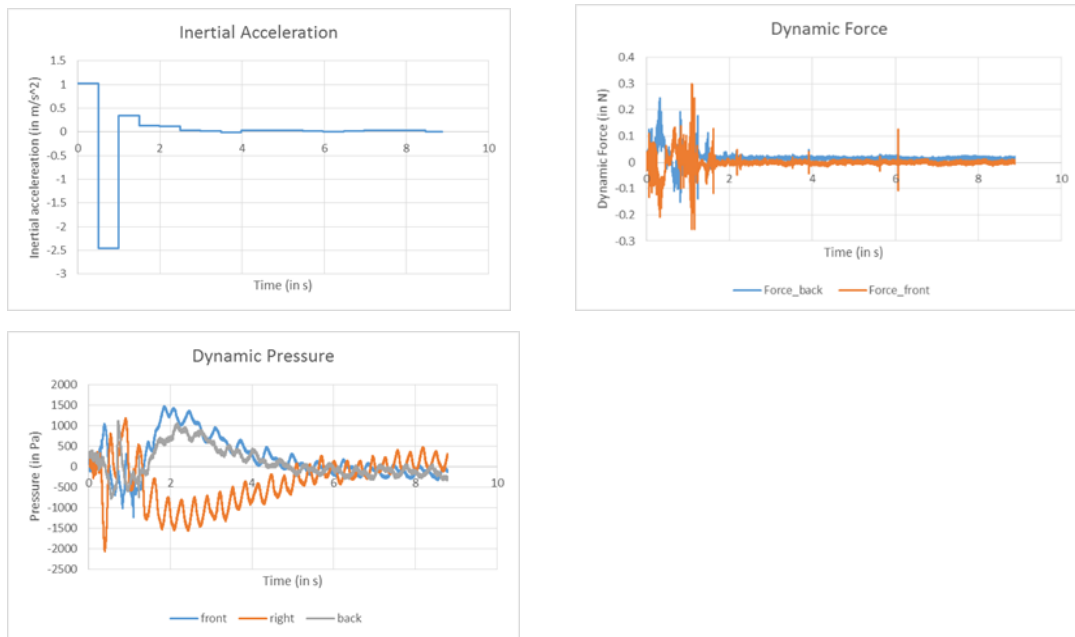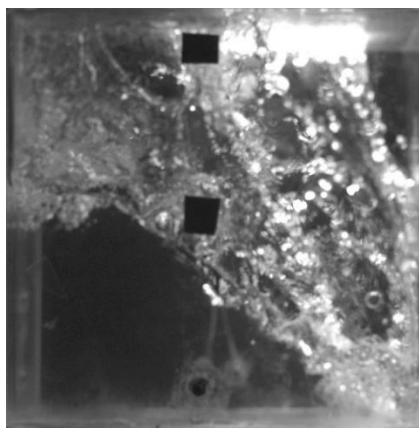
Figure 4.13: Fill level=40%, Sensor=10%, Deceleration=0.25g

However since no significant dynamic activities are taking place at the bottom of the tank and the dynamic pressure sensor recorded smaller values as compared to sensor at 30 percent of tank height. The dynamic force sensor and sensor do not show any significant change at this moment of time as there is no impact on wall.

Event 3 (1.009s)

Figure 4.14: Image Correlation: Fill level=40%, Sensor=10%, Deceleration=0.25g

Event 3 occurred when the fluid moves back towards the front wall and this movement is sensed by the sensor attached at the right wall of the tank. The

right pressure sensor shows a peak in between the two events. The part of fluid which bounced back from top surface hit the front wall at bottom near 10 % pressure sensor and hence making impact on front wall that has been sensed by all the dynamic quantities sensor at 1.009s.

After this event fluid moves again towards the rear wall hitting it at 1.237s and is detected by both the dynamic type sensor. However the amplitude is less comparable to other events.

After the two set of events the dynamic force sensors do not show any corresponding events although the dynamic pressure still shows some activity taking place inside the tank. The sloshing phenomenon inside the tank is now transitioning towards the linear sloshing regime and is well supported by high speed camera images.

Following observations can be made from the plots shown in Figure 4.11:

1st impact at rear wall: 0.732s

Dynamic Pressure=1077 Pa

Dynamic Force=0.19 N

2nd impact at front wall: 1.009s

Dynamic Pressure=308 Pa

Dynamic Force=0.32 N

Time difference in between event 1 and event 2 = 0.24s

Time difference in between event 2 and event 3 = 0. 36s

Time taken in transition from non-linear to linear sloshing =5s

Fill level =40%, sensor location =30%, Deceleration=0.3g

Inertial acceleration graph in Figure 4.15 shows that braking starts at 0.5 s and ends at 1.0s.

Acceleration jump when braking starts= 3.76m/s^2

Acceleration jump when vehicle stops= 3.47 m/s^2
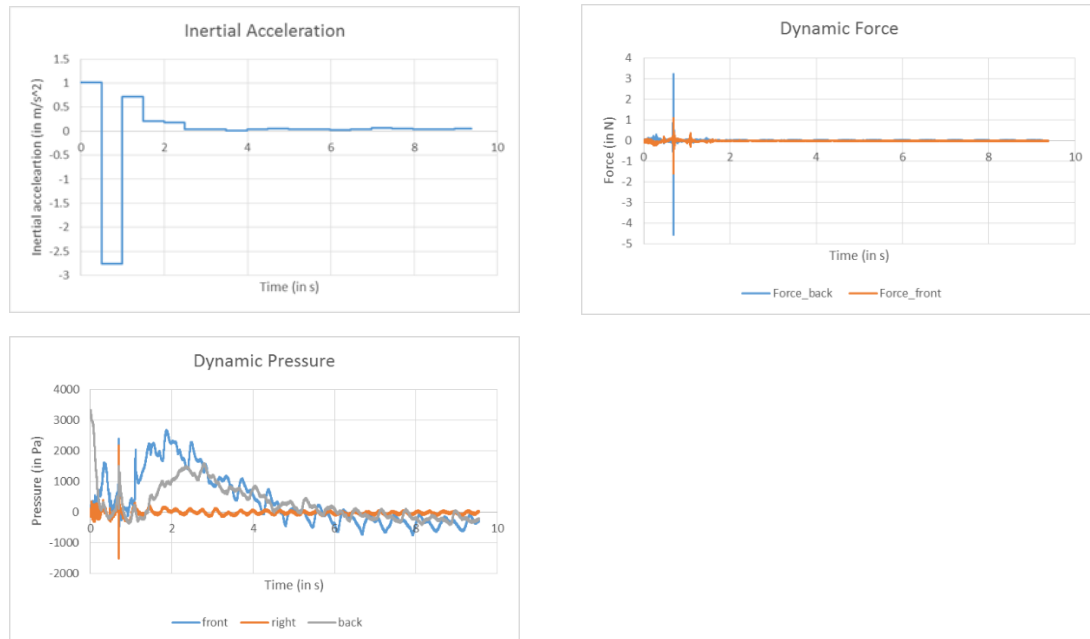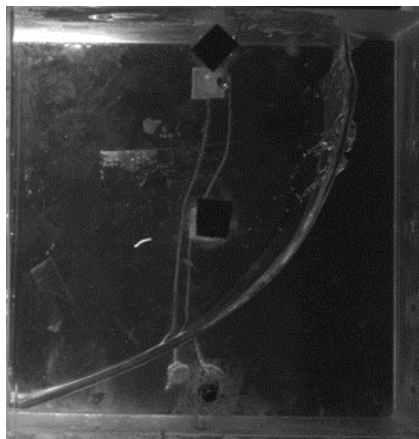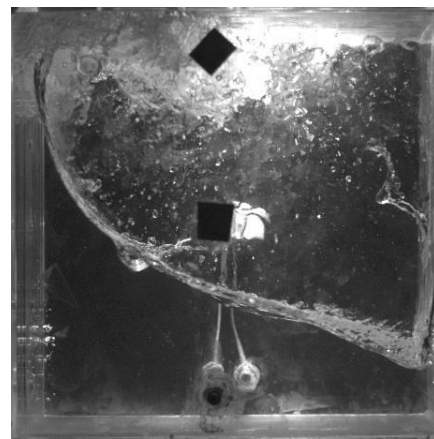

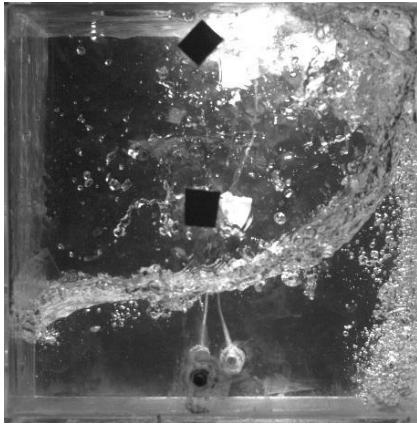**Figure 4.15: Fill level=40%, Sensor=30%, Deceleration=0.3g**

A major part of fluid has already been moved towards front wall at the time of braking as shown by high speed camera image and sensed by front dynamic pressure sensor. The movement of vehicle in opposite direction continued approximately for 0.5s.

Event 1 (0.5s)   **Event 2 (0.68s)**

Event 3 (1.04s)

Figure 4.16: Image Correlation: Fill level=40%, Sensor=30%, Deceleration=0.3g

Dynamic pressure plots show that the first hit event occurs at the rear wall which is followed by the second event at the front wall. The fluid moves towards the rear wall and smoothly climb over the rear wall and reaches maximum height at 0.694 s and this event has been captured in dynamic pressure sensor. At this moment of time the fluid has reached to the tank roof and a part of it hit the top surface and gets deflected back towards the bottom of the tank. This event is recorded in the force sensor with very high amplitude as compared to the previous case. This can be due to fluid hitting the tank roof near the rear wall created a very high impact as sensed by force sensor at 30 % of tank height. It should be noticed that at this event the force sensor at front wall has also shown a peak of low magnitude. It can be due to impact being transmitted from top surface to all the four side walls.

Event 3 occurred when themovement of the fluid back towards the front wall and this movement is sensed by the sensor attached at the right wall of the tank. The right pressure sensor shows a peak in between the two events. The fluid move upward along the front wall smoothly and hence a peak of lower magnitude is sensed by force sensor while the pressure sensor recorded a peak of significant amplitude.

After this event no clear wave hitting is seen on any of the walls. It may be due to the non-linearity present in the flow which has divided the whole flow domain in 2-3 parts which are counteracting the effects of each other. No peak is seen on force sensor although activity can be seen on pressure sensors.

This non linearity can be seen in dynamic pressure sensors. The flow becomes linear after 3-4 cycles.

Numerically,

Following observations can be made from the plots shown in Figure 4.15:

Dynamic Pressure=1508 Pa

Dynamic Force=3 N

2nd impact at front wall: 1.04s

Dynamic Pressure=2045 Pa

Dynamic Force=0.35 N

Time difference in between event 1 and event 2 = 0.19s

Time difference in between event 2 and event 3 = 0.36s

Time taken in transition from non-linear to linear sloshing =4s

Fill level =40%, sensor location =10%, Deceleration=0.3g

Inertial acceleration graph in Figure 4.17 shows that braking starts at 0.5s and ends at 1.0 s.

Acceleration jump when braking starts= 4.2 m/s^2

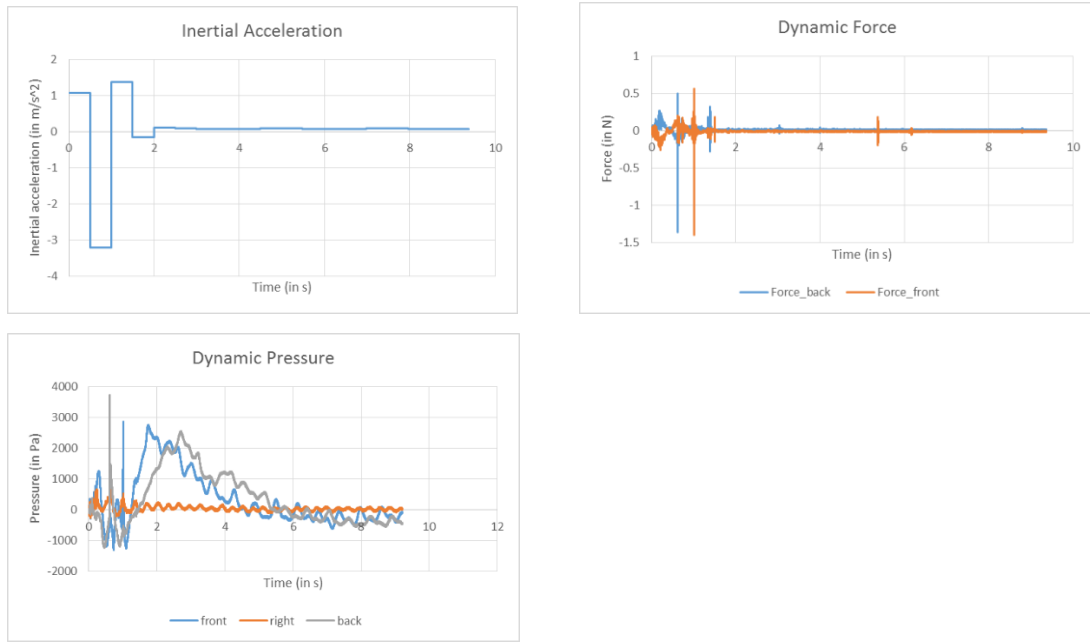Acceleration jump when vehicle stops= 4.6 m/s^2

Figure 4.17: Fill level=40%, Sensor=10%, Deceleration=0.3g

The condition at the time of braking will remain same as loading has not been changed, only the sensor position has been changed. The event 1 occurred at same time frame and the event 2 i.e. event corresponding to movement of fluid towards rear wall occurred at 0.6135s as the fluid which has moved over the front wall hit the rear wall at sensor height and makes a large impact as sensed by all the dynamic quantities sensor. After hitting the rear wall it will move along the rear wall towards the tank roof.
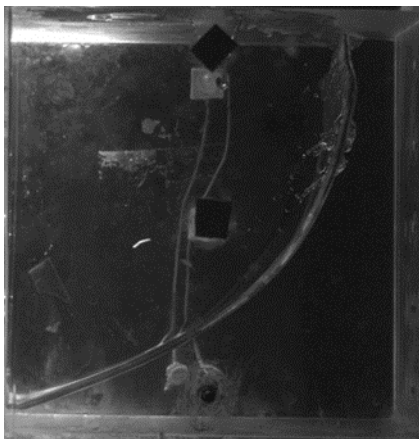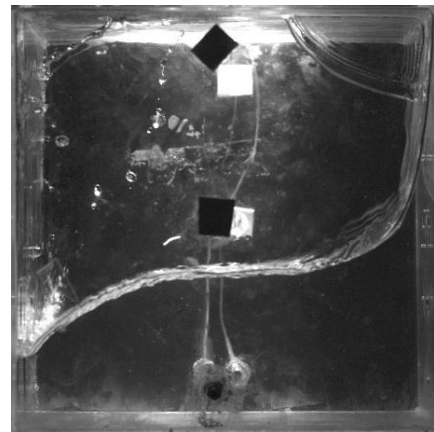
Event 1 (0.5s)   **Event 2 (0.68s)**
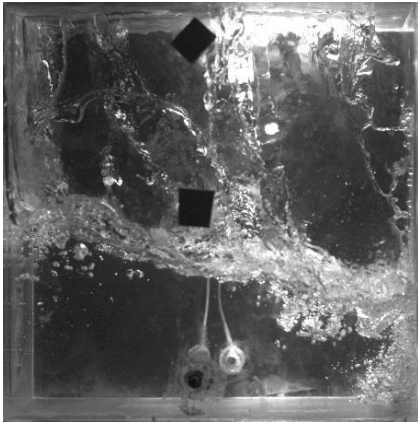
Event 3 (1.01s)

Figure 4.18: Image Correlation: Fill level=40%, Sensor=30%, Deceleration=0.3g

Event 3 occurred when the fluid moves back towards the front wall and this movement is sensed by the sensor attached at the side wall of the tank. The right pressure sensor shows an intermediate peak in between the events 2 and 3. The part of fluid which deflected back from top surface hit the front wall at bottom near 10 percent pressure sensor and made an impact on front wall that has been sensed by all the dynamic type sensor at 1.010s. This event is also sensed with larger magnitude as compared to sensor at 30 percent of tank height. This is due to fact that due to higher value of deceleration all the fluid will first accumulate toward the opposite wall and then will be making an impact at the bottom of the wall and therefore is sensed by the sensor at 10 percent of the tank height with larger magnitude.

After the two set of events the dynamic force sensors do not show any corresponding events although the dynamic pressure still shows some activity taking place inside the tank. The sloshing phenomenon inside the tank is now transitioning towards the linear sloshing regime. This is well supported by high speed camera images.

Following observations can be made from the plots shown in Figure 4.17:

1st impact at rear wall: 0.68s

49

Dynamic Pressure=3695 Pa

Dynamic Force=0.5 N

2nd impact at front wall: 1.01s

Dynamic Pressure=2853 Pa

Dynamic Force=0.56 N

Time difference in between event 1 and event 2 = 0.11s

Time difference in between event 2 and event 3 = 0. 4s

Time taken in transition from non-linear to linear sloshing =6s

Fill level =60%, sensor location =50%, Deceleration=0.2g

Inertial acceleration graph in figure 4.19 shows that braking starts at 1.0 s and ends at 1.5s.

Acceleration jump when braking starts= 2.99m/s^2

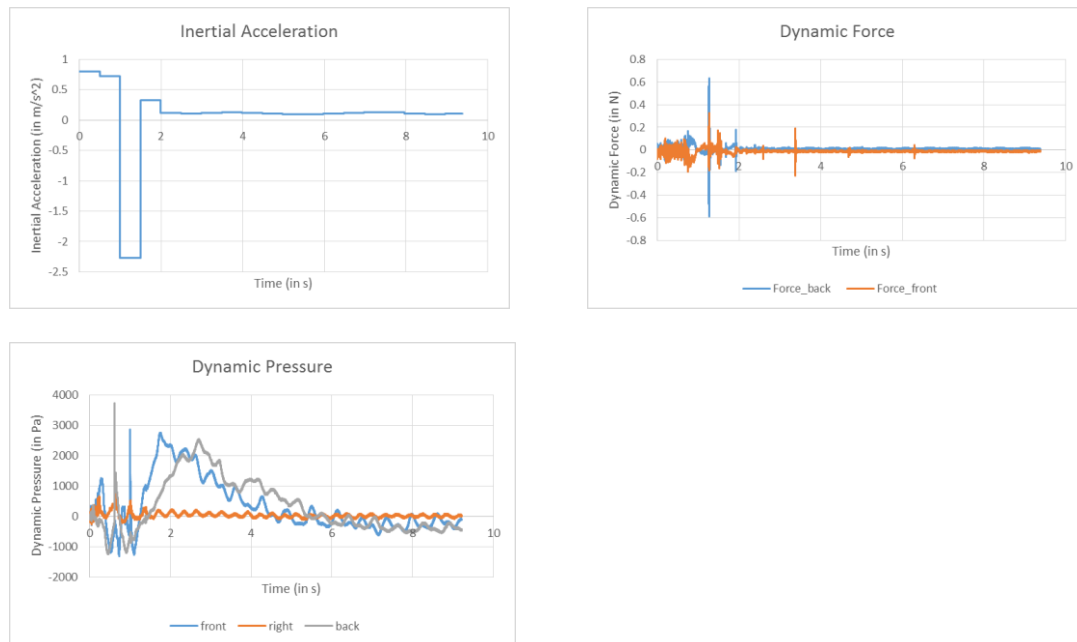Acceleration jump when vehicle stops= 2.59m/s^2

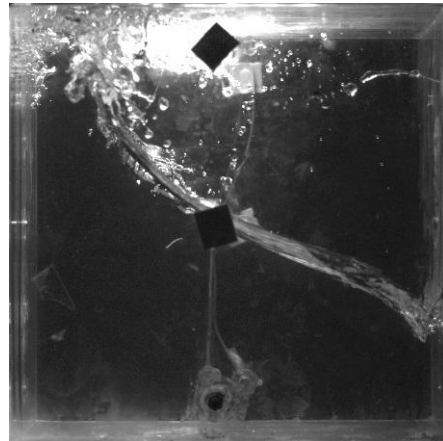Figure 4.19: Fill level=60%, Sensor=50%, Deceleration=0.2g

At the time of brake application (0.99s), high speed camera image revealed that a major part of the fluid has already moved towards the front wall and

is sensed by the pressure sensor placed on the front wall. This movement of the vehicle in the opposite direction as determined from the inertial acceleration sensor continued for 0.5s i.e. from 0.99s to 1.49s.

Dynamic pressure and dynamic force plots show that the first hit event occurred at the rear wall. The fluid moves towards the rear wall and smoothly surges over the rear wall and reaching maximum height at 1.211 s and has been captured in both dynamic type sensor. This climbing of fluid continued till water hit the tank roof and some amount of water after deflecting from the tank roof hit the front dynamic sensor and it gives a small peak.
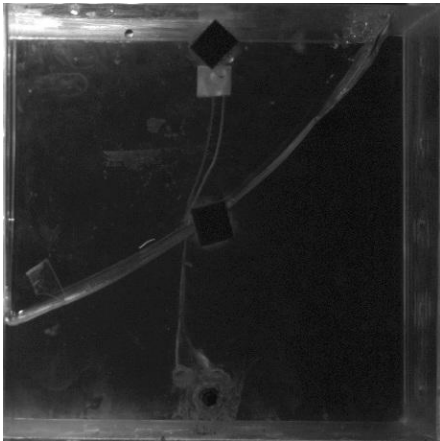
Event-1 (1.0s)

Event-2 (1.21s)
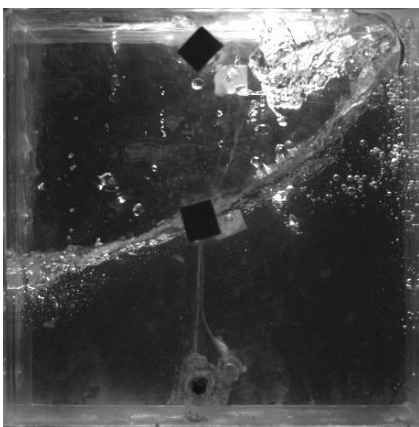
Event-3 (1.59s)

Figure 4.20: Image Correlation: Fill level=60%, Sensor=50%, Deceleration=0.2g

Event 3 occurred when the fluid moves back towards the front wall and this movement is sensed by the sensor attached at the right wall of the tank. The right pressure sensor shows an intermediate peak in between the events 2 and 3. The fluid climb along the front wall smoothly till it reaches the top and no significant activity has been recorded in dynamic force sensor. But the dynamic pressure sensor has recorded two peaks. 1st peak refers to the event when the fluid has climbed up to the maximum height it can reach while exhausting all the energy. 2nd peak is a local event and is due to some droplets of water hitting the sensor when the level of liquid is going down on the front wall and moving up on the rear wall. This event is followed by the movement of liquid towards the rear wall

After one set of events the dynamic force sensors do not show any significant events although the dynamic pressure still shows some activity taking place inside the tank. The sloshing phenomenon inside the tank is now transitioning towards the linear sloshing regime and is well supported by high speed camera.

Following observations can be made from the plots shown in Figure 4.19:

1st impact at rear wall: 1.21s

Dynamic Pressure=5251 Pa

Dynamic Force=0.621 N

2nd impact at front wall: 1.59s

Dynamic Pressure=2000 Pa

Dynamic Force=1.71 N

Time difference in between event 1 and event 2 = 0.22s

Time difference in between event 2 and event 3 = 0.38s

Time taken in transition from non-linear to linear sloshing =6s

Fill level =60%, sensor location =10%, Deceleration=0.2g

Inertial acceleration graph in figure 4.21 shows that braking starts at 1.0s and ends at 1.5s.

Acceleration jump when braking starts= 2.69 m/s^2

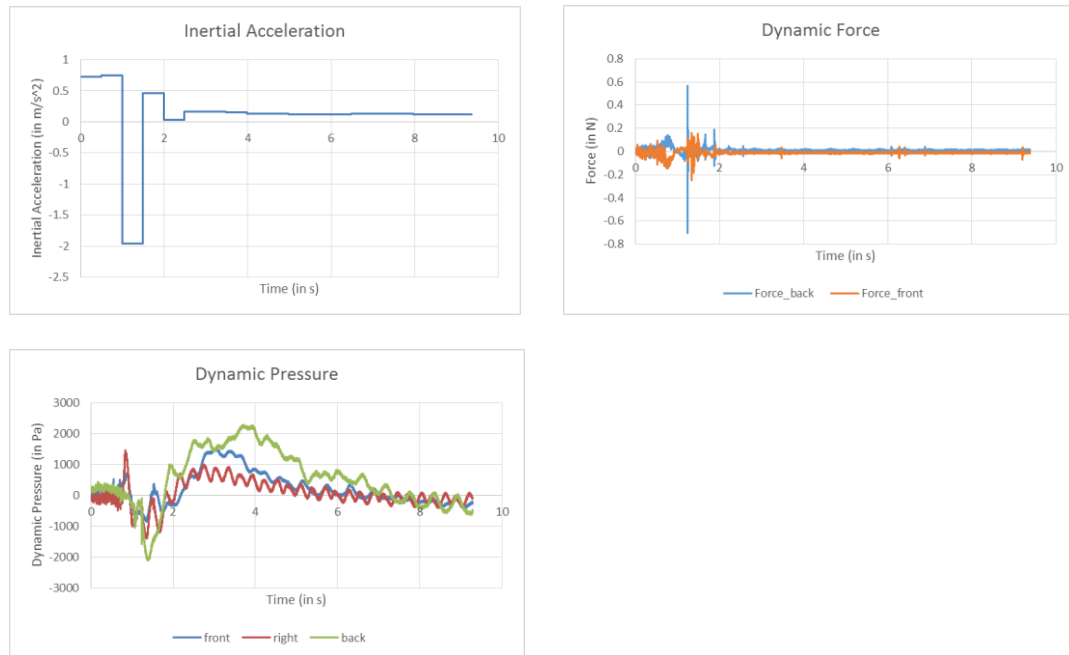Acceleration jump when vehicle stops= 2.41 m/s^2

Figure 4.21: Fill level=60%, Sensor=10%, Deceleration=0.2g

The condition at the time of braking will remain same as loading has not been changed, only the sensor position has been changed. The event 2 will occur at same time frame but no activity is seen by the dynamic pressure sensor at rear wall, however peak of significant amplitude is shown by force sensor. This is due to the fact that pressure sensor being in direct contact with the fluid do not see any corresponding dynamic changes at 10 % of tank height when the fluid level is 60% but the dynamic force sensor record significant peaks which are of same magnitude as recorded when the sensor were placed at 50% of tank height. This is because these sensors record the wall vibration which will be same in both cases.
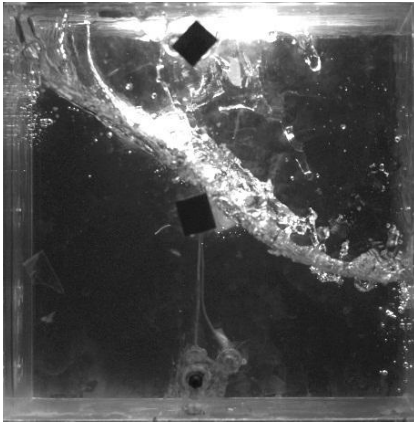
Event-3 (1.35s)

Figure 4.22: Image Correlation: Fill level=60%, Sensor=10%, Deceleration=0.2g

The event 3 i.e. event corresponding to movement of fluid towards front wall occur at 1.35s when the fluid moves towards the front wall and hits the front wall at certain height from sensor location. But the impact of hit is not recorded as the sensor location is significantly below the point of hit. The dynamic force sensor do not show any significant change at this moment of time.

This event is followed by the movement of the fluid towards rear wall. This location of sensor cannot be used to predict the time period taken by the fluid to come under the linear sloshing regime. This is due to the fact that sensor at this location are not recording any dynamic activity

Following observations can be made from the plots shown in Figure 4.19:

1st impact at rear wall: 1.21s

Dynamic Pressure=89 Pa

Dynamic Force=0.57 N

2nd impact at front wall: 1.34s

Dynamic Pressure=250 Pa

Dynamic Force=0.15 N

Time difference in between event 1 and event 2 = 0.21s

Time difference in between event 2 and event 3 = 0. 13s

Fill level =60%, sensor location =50%, Deceleration=0.25g

Inertial acceleration graph in figure 4.23 shows that braking starts at 0.5 s and ends at 1.0s.

Acceleration jump when braking starts= 3.59m/s^2.

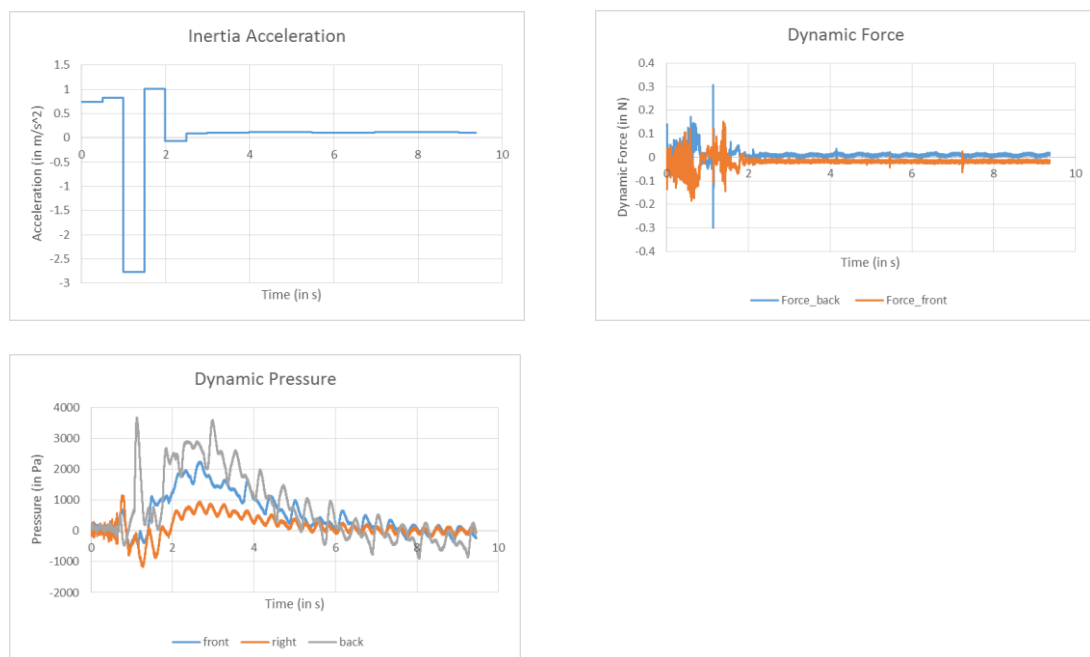Acceleration jump when vehicle stops= 3.78m/s^2

Figure 4.23: Fill level=60%, Sensor=50%, Deceleration=0.25g

At the time of brake application (0.99s), high speed camera image revealed that a major part of fluid has already moved towards the front wall. The movement of vehicle in opposite direction as described from the inertial acceleration sensor continued for approximately 0.5s i.e. from 0.99s to 1.49s.
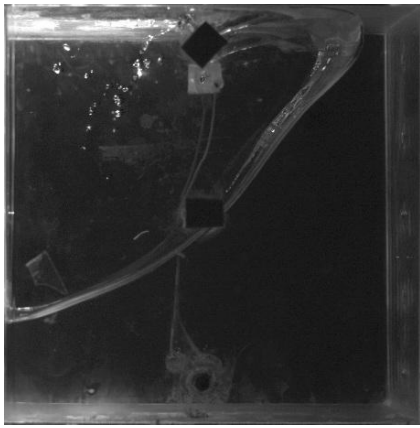
Event-1 (1.0s)
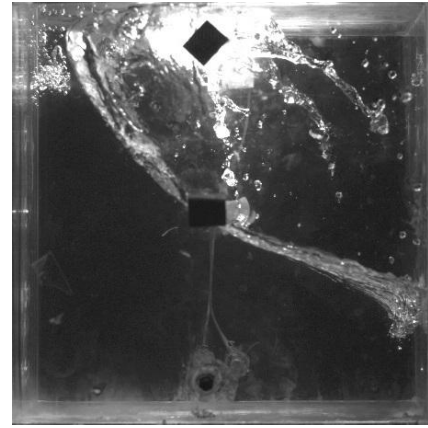
Event-2 (1.127s)

Event-3 (1.48s)

Figure 4.24: Image Correlation: Fill level=60%, Sensor=50%, Deceleration=0.25g

Dynamic pressure plots show that the first hit event occurs at the rear wall which is followed by the second event at the front wall.

The fluid moves towards the rear wall and smoothly surge over the rear wall and reaching maximum height at 1.145 s and this event has been captured in dynamic quantities sensor. At this moment of time the fluid has reached to tank roof and a part of it hit the top surface and deflected back towards the bottom of tank.

Event 3 occurred when the fluid moves back towards the front wall. The fluid hits the front wall and makes an impact on the wall and this event has been captured in both the dynamic type sensors. But the amplitude of peak

recorded is lower as compared to impact at rear wall. This may be due to a large amount of air packets associated with this effect. The fluid moves towards the rear wall and a peak is recorded by the dynamic pressure sensor at rear wall..

After two set of events the dynamic force sensors do not show any significant corresponding events although the dynamic pressure still shows some activity taking place inside the tank. The sloshing phenomenon inside the tank is now transitioning towards the linear sloshing regime. This is well supported by high speed camera images.

Following observations can be made from the plots shown in Figure 4.23:

1st impact at rear wall: 1.127s

Dynamic Pressure=3700 Pa

Dynamic Force=0.3 N

2nd impact at front wall: 1.48s

Dynamic Pressure=1100 Pa

Dynamic Force=0.15 N

Time difference in between event 1 and event 2 = 0.127s

Time difference in between event 2 and event 3 = 0.335s

Time taken in transition from non-linear to linear sloshing =6s.

Fill level =60%, sensor location =10%, Deceleration=0.25g

Inertial acceleration graph in figure 4.25 shows that braking starts at 1.0s and ends at 1.5s.

Acceleration jump when braking starts= 3.14 m/s^2

Acceleration jump when vehicle stops= 3.36 m/s^2

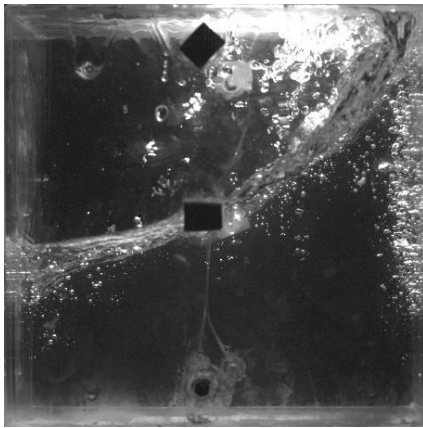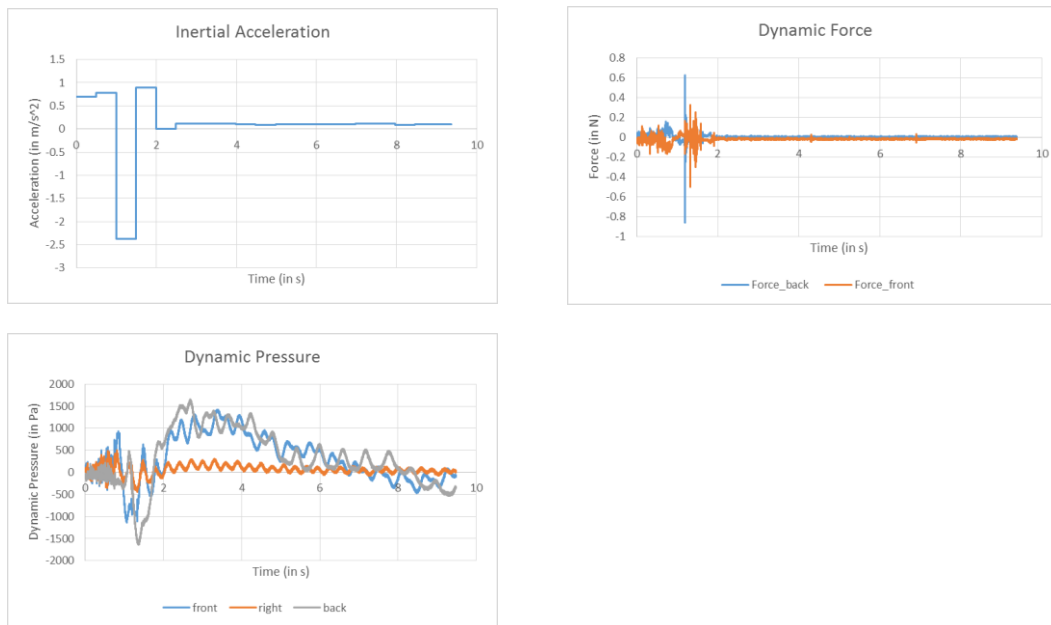**Figure 4.25: Fill level=60%, Sensor=10%, Deceleration=0.25g**

The condition at the time of braking will remain same as loading has not been changed, only the sensor position has been changed. The event 1 will occur at same time frame and the event 2 i.e. event corresponding to movement of fluid towards rear wall will also occur at same time as the transition of fluid was smooth and no impact was observed. However since no significant dynamic activities are taking place at the bottom of the tank and the dynamic pressure sensor will just record change in fluid level and this value will be small as compared to sensor at 50 percent of the tank height. The dynamic force sensor record this events as they are placed on the outer side of the wall and are meant for recording wall vibrations.

Event 3 occurred when the fluid moves back towards the front wall. The part of fluid which bounced back from top surface and the fluid coming from the rear wall will move smoothly over the front wall and this smooth climbing is sensed by dynamic pressure sensor on front wall at 1.48s. This event is not recorded significantly in force sensor as there is no significant impact taking

58

place. After this event fluid moves again towards the rear wall hitting it at 1.98s.

After the two set of events the dynamic force sensors do not show any corresponding events although the dynamic pressure still shows some activity taking place inside the tank. The sloshing phenomenon inside the tank is now transitioning towards the linear sloshing regime.

Following observations can be made from the plots shown in Figure 4.23:

1st impact at rear wall: 1.13s

Dynamic Pressure=488 Pa

Dynamic Force=0.6 N

2nd impact at front wall: 1.48s

Dynamic Pressure=582 Pa

Dynamic Force=0.35 N

Time difference in between event 1 and event 2 = 0.18s

Time difference in between event 2 and event 3 = 0. 3s

Time taken in transition from non-linear to linear sloshing =5.5s

Fill level =60%, sensor location =50%, Deceleration=0.3g

Inertial acceleration graph in Figure 4.26 shows that braking starts at 1.0 s and ends at 1.5s.

Acceleration jump when braking starts= 4.2m/s^2

Acceleration jump when vehicle stops= 4.7 m/s^2

At the time of brake application (0.49s), high speed camera image revealed that a major part of fluid has already moved towards the front wall. After brake application the movement of vehicle in opposite direction as determined from the inertial acceleration sensor continued for 0.5s.
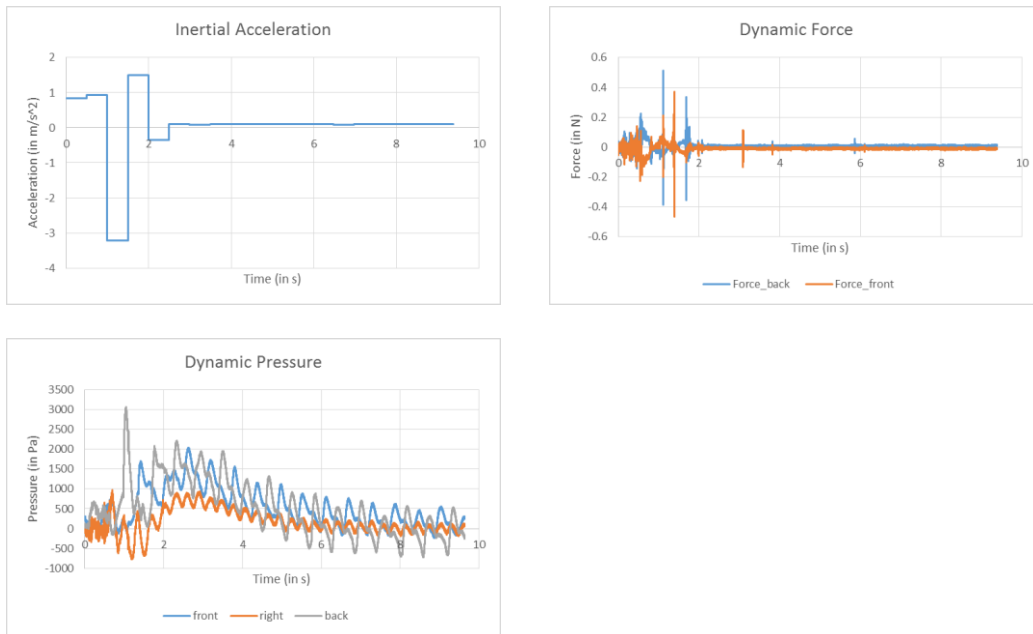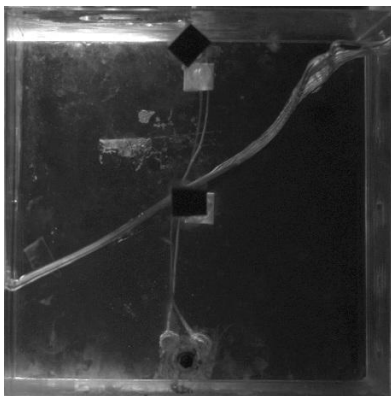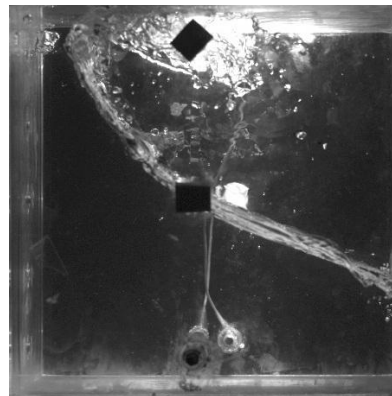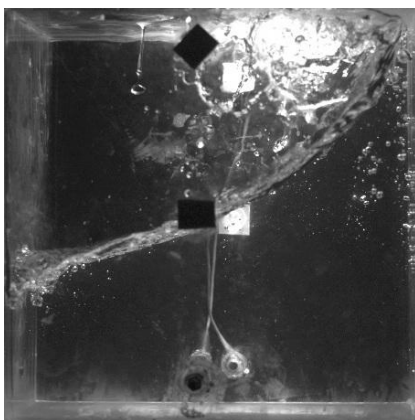
Figure 4.26: Fill level=60%, Sensor=50%, Deceleration=0.3g

Event-1 (0.5s)

Event-2 (1.1s)

Event-1 (1.4s)

Figure 4.27: Image Correlation: Fill level=60%, Sensor=50%, Deceleration=0.3g

60

Dynamic pressure plots show that the first hit event occurred at the rear wall which is followed by the second event at the front wall.

The fluid moves towards the rear wall and smoothly surge over the rear wall and reaching maximum height at 1.044 s and this event has been captured in dynamic pressure sensor. At this moment of time the fluid reached the tank roof and a part of it hit the top surface and deflected back towards the bottom of tank. This event is recorded in force with a high amplitude. This can be due to fluid hitting the tank roof near the rear wall with very high velocity thus creating very high impact as sensed by force sensor at 50 % of tank height. It should be noticed that at this event the force sensor on front side has also shown a peak of low magnitude. It can be due to impact being transmitted from top surface to all the four side walls.

Event 3 occurred when the fluid moves back towards the front wall and this movement is sensed by the sensor attached at the side wall of the tank. The fluid surge the front wall smoothly and hits the top surface. A peak of lower magnitude has been sensed by force. Dynamic pressure sensor show a smaller peak as there is no impact associated with this event.

After this event no clear wave hitting is seen on any of the walls. It may be due to the non-linearity present in the flow. No peak is seen on force sensor although activity can be seen on pressure sensors.

This non linearity can be seen in dynamic pressure sensors. The flow become linear after 3-4 cycles.

Following observations can be made from the plots shown in Figure 4.26:

1st impact at rear wall: 1.1 s

Dynamic Pressure=3048 Pa

Dynamic Force=0.515 N

2nd impact at front wall: 1.4s

Dynamic Pressure=1703 Pa

Dynamic Force=0.37 N

Time difference in between event 1 and event 2 = 0.1s

Time difference in between event 2 and event 3 = 0.3s

Time taken in transition from non-linear to linear sloshing =5s.

Fill level =60%, sensor location =10%, Deceleration=0.3g

Inertial acceleration graph in figure 4.28 shows that braking starts at 1.0s and ends at 1.5s.

Acceleration jump when braking starts= 4.2 m/s^2

Acceleration jump when vehicle stops= 4.65 m/s^2

The condition at the time of braking will remain same as loading has not been changed, only the sensor position has been changed. The event 1 occurred at same time frame and the event 2 i.e. event corresponding to movement of fluid towards rear wall occurred at 1.10s as the fluid has moved in upward direction smoothly along rear wall and hit the roof as recorded by dynamic force sensor. The pressure sensor has not sensed any significant peak as there was no dynamic event taking place inside the tank at 10% of tank height.
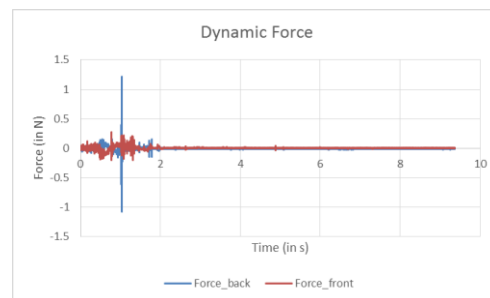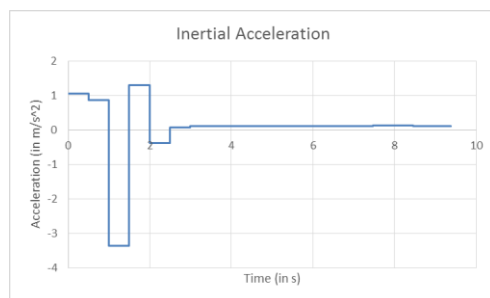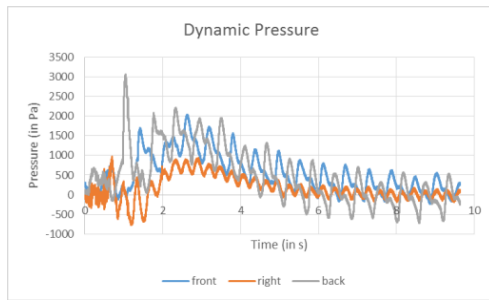
Figure 4.28: Fill level=60%, Sensor=10%, Deceleration=0.3g

Event 3 occurred when fluid moves back towards the front wall and this movement is sensed by the sensor attached at the side wall of the tank. Not much dynamic activity is taking place near the bottom as observed in the high speed camera image and no activity is recorded in dynamic type sensor.

After the one set of event the dynamic pressure and dynamic force sensors do not show any corresponding events. No conclusion can be made for linearity of sloshing using analysis at 10% of sensor height as these sensors do not record any dynamic events.

Following observations can be made from the plots shown in Figure 4.28:

1st impact at rear wall: 1.10 s

Dynamic Pressure=583 Pa

Dynamic Force=1.2 N

2nd impact at front wall: 1.35s

Dynamic Pressure=284 Pa

Dynamic Force=0.2 N

Time difference in between event 1 and event 2 = 0.10s

Time difference in between event 2 and event 3 = 0. 25s

Fill level =80%, sensor location =70%, Deceleration=0.25g

Inertial acceleration graph shows that braking starts at 1.0 s and ends at 1.5s.

Acceleration jump when braking starts= 3.43 m/s^2

Acceleration jump when vehicle stops= 3.73m/s^2

The condition of fluid inside the tank at the time of first event at front dynamic pressure sensor when analyzed from high speed camera image revealed that a major part of fluid has moved towards the front wall. After brake application the vehicle will move some distance opposite to direction of motion due to elasticity of string used for brake application. This movement of vehicle as described from the inertial acceleration sensor continued for 0.5s i.e. from 0.99s to 1.49s.
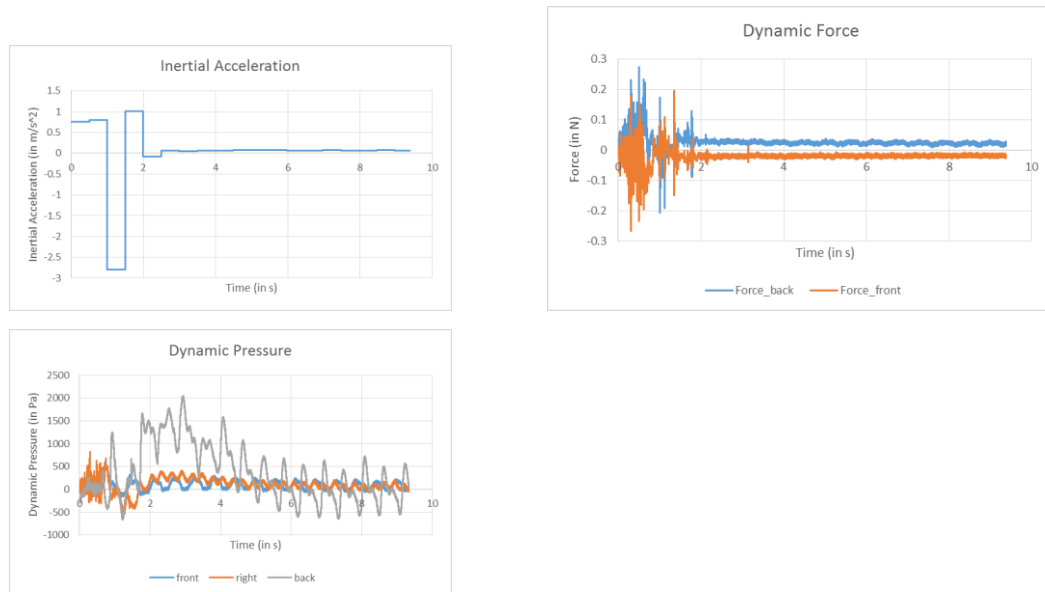
Figure 4.29: Fill level=80%, Sensor=70%, Deceleration=0.25g

Dynamic pressure plots show that the first hit event occurs at the rear wall which is followed by the second event at the front wall.

The fluid moves towards the rear wall and hits the rear wall and makes an impact at 0.91 s and this event has been captured in dynamic pressure sensor

and dynamic force sensor. This hitting is accompanied by fluid moving along the roof of the tank towards the front wall.
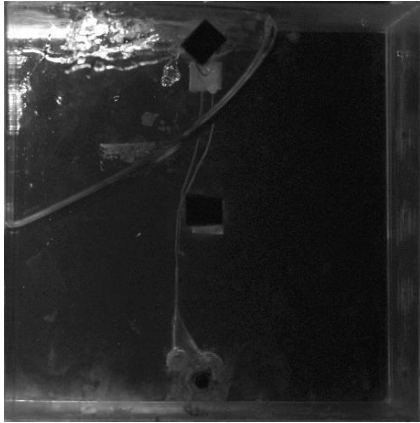
Event-1 (0.7s)
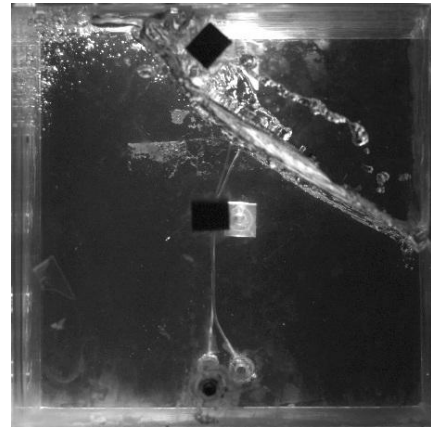
Event-2 (0.91s)
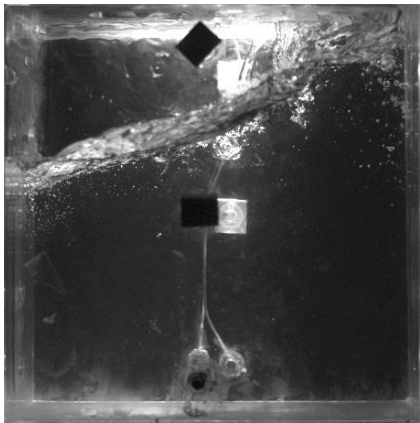
Event-3 (1.43s)

Figure 4.30: Image Correlation: Fill level=60%, Sensor=50%, Deceleration=0.25g

Event 3 occurred when the movement of the fluid back towards the front wall. The fluid surges the front wall smoothly and hence no significant peak is shown in front pressure sensor. However the force sensor has shown some activity at the front wall. The force sensor has shown the peak due to fluid hitting the roof of the tank. It is clear from the high speed camera images that fluid smoothly climbed upon the front wall and makes no direct hit on front wall and hence no dynamic activity is shown by front pressure sensor. After this fluid moved towards the rear wall making an impact on the rear wall at 1.57s.

This case is accompanied by very low dynamic activities on the front wall as recorded by dynamic pressure sensor located at front wall.

After two set of events the dynamic force sensors do not show any significant corresponding events although the dynamic pressure at rear wall still shows some activity taking place inside the tank.

Numerically,

1st impact at rear wall: 0.9 s

Dynamic Pressure=2836 Pa

Dynamic Force=0.16 N

2nd impact at front wall: 1.43s

Dynamic Pressure=530 Pa

Dynamic Force=0.21 N

Fill level =80%, sensor location =10%, Deceleration=0.25g

Inertial acceleration graph shows that braking starts at 1.0s and ends at 1.5s.

Acceleration jump when braking starts= 3.46 m/s^2

Acceleration jump when vehicle stops= 3.72 m/s^2
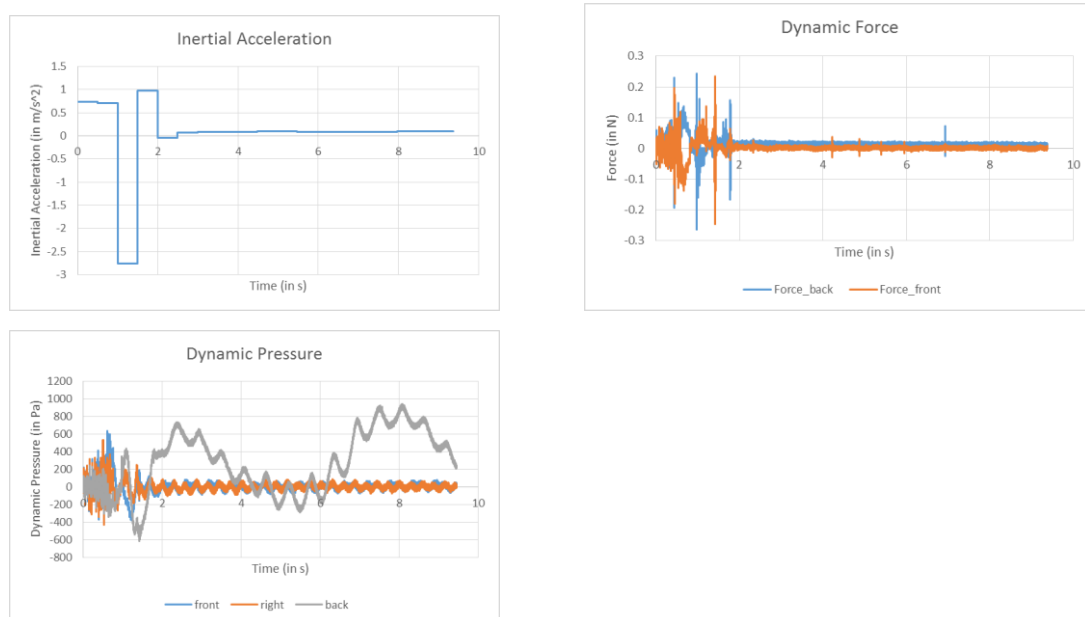
Figure 4.31: Fill level=80%, Sensor=10%, Deceleration=0.25g

The condition at the time of braking will remain same as loading has not been changed, only the sensor position has been changed. The event 1 will occur at same time frame and the event 2 i.e. event corresponding to movement of fluid towards rear wall occur at 1.0847 s when the fluid has moved towards the rear wall and has just started to revert back towards front wall.

The event 2 is followed by movement of fluid towards front wall. This will occur at same time as it occurred for sensor location of 70%. This is because even the front dynamic pressure sensor located at 70% of tank height is not facing any dynamic effects.

After the two set of events the dynamic pressure and dynamic force sensors do not show any corresponding events although the dynamic pressure still shows some activity taking place inside the tank. But the front and right pressure sensor do not show any significant changes and the changes in back pressure sensor values are also very low which means that at this location of sensor no dynamic activity is taking place and hence we can't comment about time taken by the fluid to come under linear sloshing zone.

Numerically,

1st impact at rear wall: 0.91s

Dynamic Pressure=434 Pa

Dynamic Force=0.2 N

2nd impact at front wall: 1.43s

Dynamic Pressure=189 Pa

Dynamic Force=0.23 N

The things that can be concluded from the study based on variation in load:

i. Dynamic force and dynamic pressure plots show that the first event occurs at the rear wall which is followed by the second event at the front wall.

ii. As we increase the load, time taken for sloshing to become linear increases as it took 6.5s to become linear when the deceleration was 0.3g.

iii. At higher load splash comes into picture as activity in the center increases but contribution of splash is not significant in the noise.

4.2 Flow Regimes

Analysis of data from front and back dynamic pressure sensor recorded during experiments suggested that two flow regimes were present during every experiment which are as follows:

i. Non-linear Flow Regime

ii. Linear flow Regime

Non-linear flow regime can be again classified into impact zone also termed as strongly non-linear zone and transition zone or weakly non-linear zone.

Impact Zone: This non linearity is mainly due to rapid velocity changes associated with hydrodynamic pressure impacts of the liquid motion close to the free surface. This zone dominates for first few cycles of sloshing phenomenon and the number of cycles depend upon fill level and deceleration value. This type of non-linearity is recorded in the form of peaks on front and rear walls and is associated with high value of impact force on walls as recorded by dynamic force sensor.

Transition Zone: This type of nonlinearity arises due to oscillations of large amplitude in which the free liquid surface experiences non-planar motion. In dynamic pressure sensor data this region can be identified as region where the pressure value decays gradually from peak towards the linear regime.

Linear Zone: This regime is associated with small oscillations of fluid free surface in which the surface remains planar without rotation. This regime is recorded in the form of smooth waves in pressure sensors.

These flow regimes were observed in high speed camera images as shown in Figure 4.32 and have been represented in dynamic pressure data as shown in Figure 4.33

Depending upon the deceleration value and fill levels, the duration of three regimes varies. For larger deceleration value, the impact regime will be of longer duration as the flow non linearity will be more due to presence of bubbles and air packets in the flow.
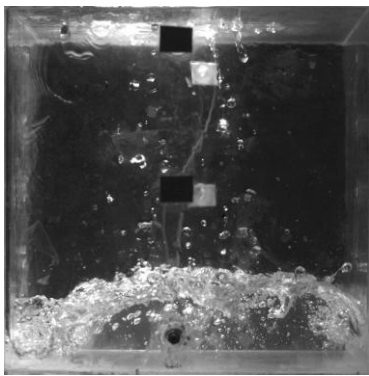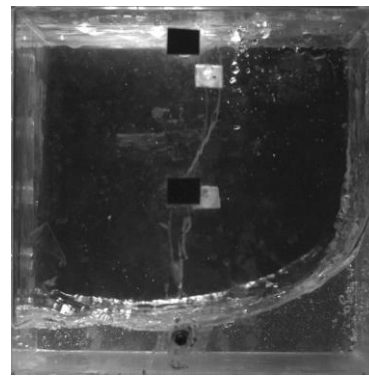
Impact Flow Regime   **Transition Flow Regime**
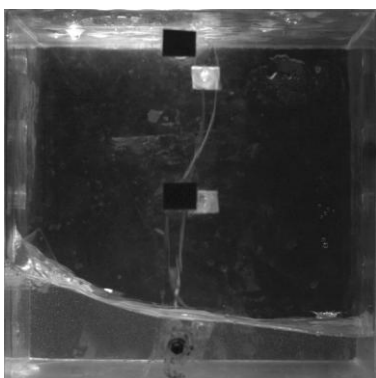
Linear Flow Regime

Figure 4.32: Different flow regimes as observed from high speed camera images.
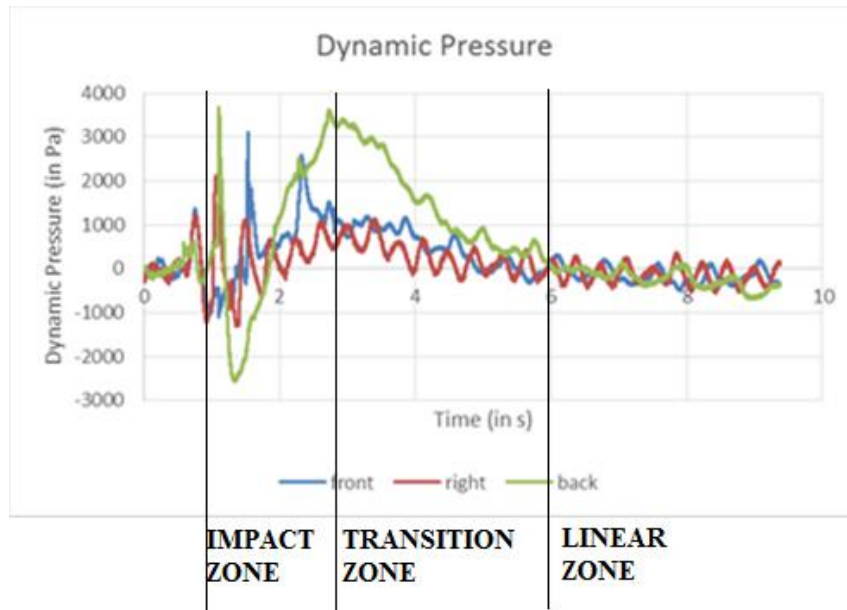
Figure 4.33: Different flow regimes in Dynamic Pressure Data.

4.3 Observations

4.3.1 Effect of Fill level

In order to check the effect of fill level on dynamic force and dynamic pressure for a constant deceleration, this study was done. Figure 4.34 show the plots for this study. Figure A refers to dynamic pressure plot with respect to fill level. For deceleration of 0.2g, it was observed that dynamic pressure at front and rear wall is similar, for 40% fill level dynamic pressure at front wall has recorded a higher value while for 60% fill level dynamic pressure at back sensor has recorded higher value. This is because for 20% fill level, wave front impact takes place on both the walls. In case of 40% fill level, liquid surges smoothly over the back wall but it makes an impact on front wall while for 60% fill level, the liquid climbs over the back wall smoothly and then moves towards the front wall and on front wall also the climbing of liquid over wall is smooth. The difference in two pressure magnitudes is because first interaction after wall will comprise more dynamic activity then second interaction at wall. As can be observed from the figure for deceleration of 0.25g and 0.3g, dynamic

pressure at rear wall is higher as compared to dynamic pressure at front wall for fill level of 20%, 60% and 80% but for 40% of fill level, dynamic pressure at front wall dominates over dynamic pressure at back wall.

For fill level of 20%, the event 2 and event 3 which are defined as events at rear wall and front wall respectively are impact events where the liquid hits the wall violently. But for higher fill levels, impact takes place either at certain height from the probe location or at the tank roof. Fill level of 40% is intermediate fill level in which event at rear wall is the smooth movement of fluid along the wall in upward direction and hit at tank roof while event 3 refers to impact on front wall in vicinity of sensor. This is the reason why dynamic pressure sensor at front wall show a higher peak as compared to dynamic pressure sensor at back wall.

Fill levels of 60% and 80% are associated with surging of fluid towards tank roof and hitting the roof but 80% fill is associated with more rigid mass and hence dynamic activity inside the fluid will be low as compared to 60%. Hence the peak for 60% is larger than 80%.

Effect of Fill level on Dynamic Pressure for Deceleration =0.25g

Effect of Fill Level on Dynamic Force for Deceleration=0.25g

Effect of Fill level on Dynamic Pressure for Deceleration=0.3g

Effect of Fill Level on Dynamic Force for Deceleration=0.3g
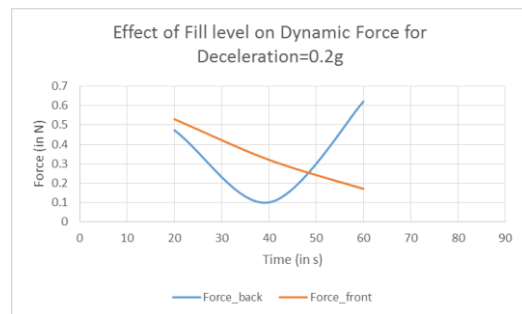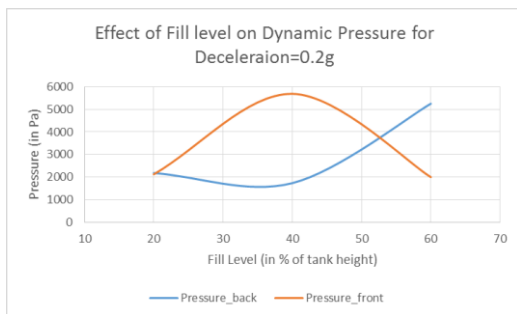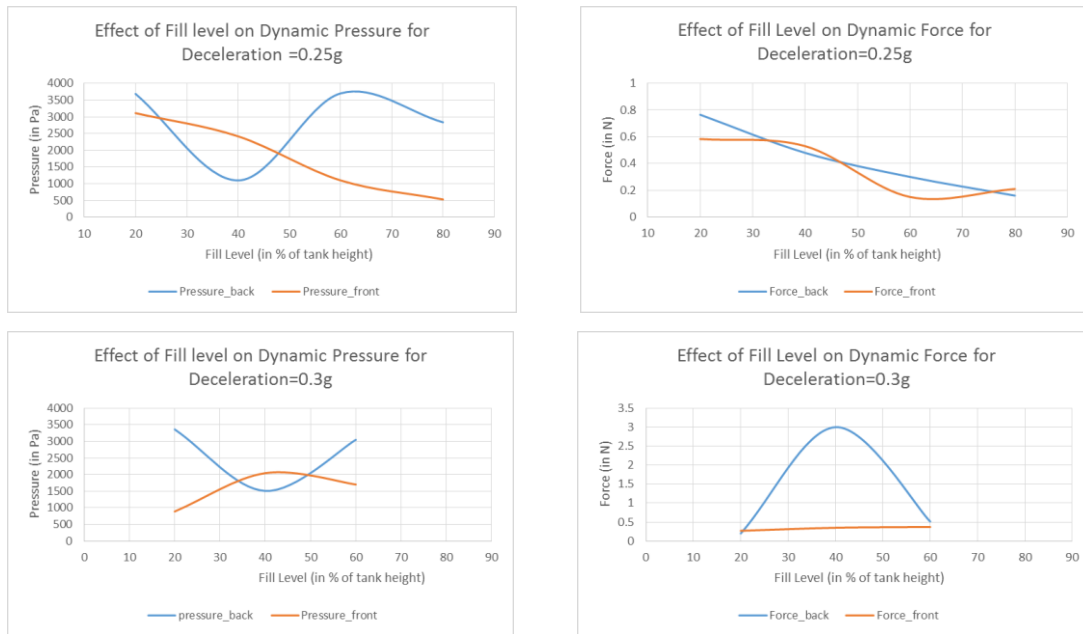
A. Dynamic Pressure Plot   **B. Dynamic Force Plot**

Figure 4.34 Effect of fill level for constant g

Analysis of effect on dynamic force for fill level of 0.2g showed trend similar to dynamic pressure plot. Plots for 0.25g showed that the dynamic force at rear wall is higher than dynamic force at front wall for fill level of 20%, 60% and 80% and front force is higher for 40% which is similar to trend observed in dynamic pressure sensor. However it should be noticed that at 80% of fill level although difference in dynamic pressure for two boundaries is large but they show similar dynamic force for both the events. This is due to the fact that at higher fill level, liquid surges along the wall and hit the tank roof. There is no direct hit either on front wall or on rear wall for 80% of fill level. For deceleration of 0.3g, it can be observed that for 40% of fill level, the force at rear sensor has recorded a peak force of 3N. This event occurred when the fluid has hit the roof top violently and this event is characterized by a noise of around 75dB.

72

4.3.2 Effect of Deceleration:

A study was done to observe the effect of deceleration value for a constant fill level. The fill level taken under consideration was 20% of tank height. Figure 4.35 show the plots for effect on dynamic pressure and effect on dynamic force.
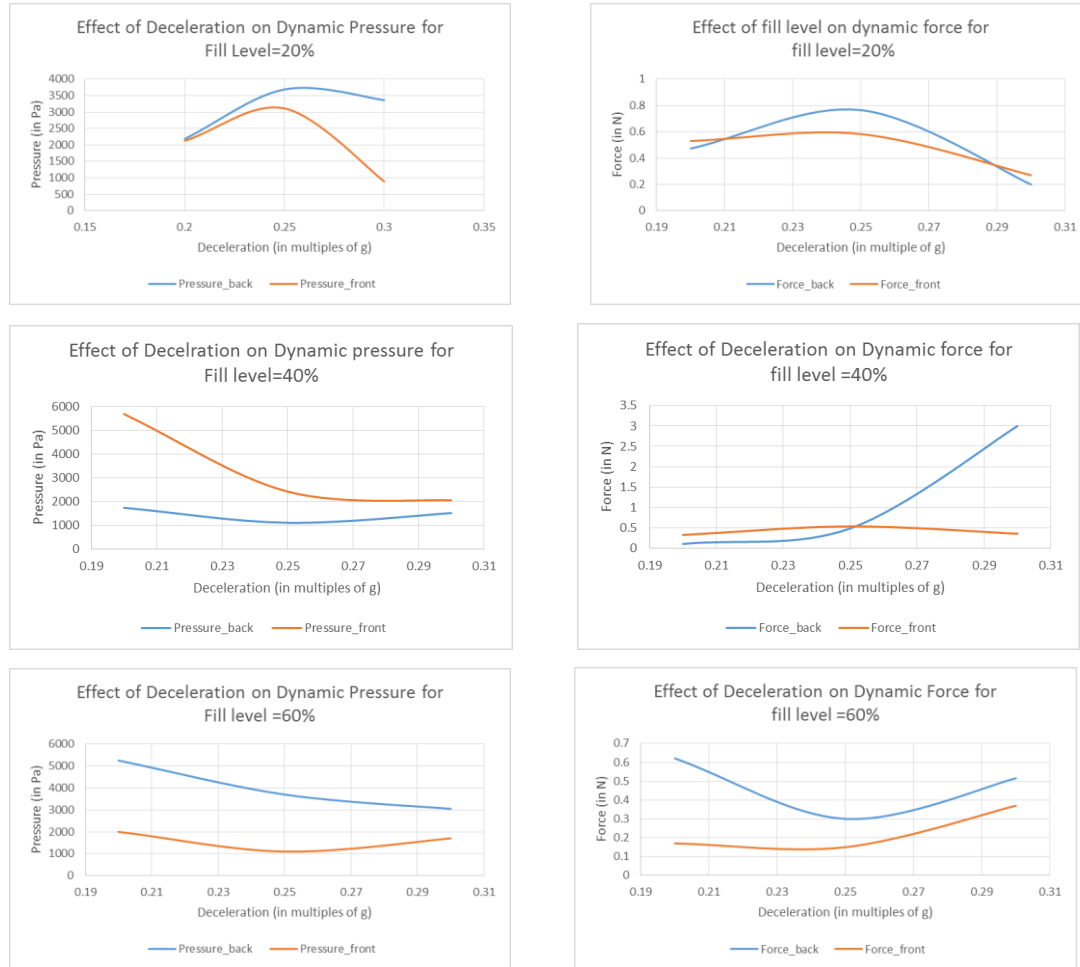
| A. Dynamic Pressure Plot | B. Dynamic Force Plot |

Figure 4.35 Effect of deceleration for fill level=20%

It can be observed from dynamic pressure and dynamic force for 20% of fill level plot that both pressure and force are maximum for deceleration of 0.25g. At 0.3 g due to entrapment of air the pressure at rear wall has reduced as compared to 0.25g. For deceleration of 0.3g, during event at the rear wall, a significant amount of fluid climb along the rear wall and falls near the front wall of the tank. The remaining liquid travels forward towards the front wall.

This liquid wave interacts with the liquid that is dropping from the roof of the tank. This interaction occurs near the front dynamic pressure sensor and therefore its response gets reduced.

Dynamic Pressure plot for fill level of 40% showed that at 0.2g the front sensor at front recorded higher value than for rear pressure sensor. This is due to the reason that liquid surges smoothly over back wall while it moves back and hit the wall making an impact during event at front wall. For other decelerations the difference in recorded pressure for two sensors is low as the event at rear wall is associated with smooth surging of fluid while liquid hits at certain height from sensor location during event at front wall.

Events for Fill level of 60% are events when the fluid surges on the wall smoothly reaching tank roof. Dynamic pressure for rear wall sensor is always higher than dynamic pressure for front wall sensor. This is because during second interaction with wall, energy associated with the flow is lower as compared to front interaction and also the flow will be more non-linear during second interaction. The peak pressure has reduced with increase in deceleration as the extent of non-linear behavior and entrapped bubble is also increased with increase in deceleration.

Dynamic force plot also show the same behavior for different fill levels. For fill level of 20%, the force at front wall is higher than force at rear wall unlike pressure plots for deceleration of 0.3g. This is because the wave front hits the front wall at certain height from the sensor location but this hit is recorded by dynamic force sensor as it records the vibration of wall due to hit as a whole. For fill level of 40% and 60%, dynamic force follow the same behavior as recorded by dynamic pressure sensors for lower decelerations, but for deceleration of 0.3g, 40% fill level has shown a peak of 3N at rear pressure

sensor. This instant is characterized by liquid hitting the tank roof violently after surging along the wall.

4.3.3 Effect of sensor location:

The location of dynamic type sensors was varied and they were placed at 10% of tank height and 10% below the free surface for each set of fill level and deceleration value. The observations made from this study are:

i. The sensors at 10% of tank height do not experience any dynamic activity for 60% and 80% case while they experience some activity for 40% case when the deceleration value is 0.3g.

ii. The force sensor sense the overall activity taking place on the wall. This is the reason when the fluid hits the roof of the tank dynamic pressure sensor do not show any peak.

iii. The peak at front dynamic pressure sensor at the time of brake will be recorded in sensor at 10% of tank height and sensor at 10% below the fill level at same time as this is the time when fluid is climbing smoothly on the front wall thus sensors will experience change in static pressure.

4.3.4 Non Linear sloshing and linear sloshing duration:

Sloshing phenomenon observed during experimentation can be differentiated broadly in two regimes:

i. Non-linear sloshing regime

ii. Linear Sloshing regime

Application of brake is associated with movement of fluid towards the front wall and this event is linear as this movement is smooth and hence is recorded by front dynamic pressure sensor. After this event the fluid reaches maximum height and then moves towards the rear wall and make an impact on it and is

followed by an impact on front wall. These two impacts comes under strongly non-linear regime. High speed camera images at these two events show entrapment of air in liquid which make the flow non-linear.

The impact regime is followed by the transition regime and is characterized by bubbly flow. This is weekly non-linear flow regime and is associated with oscillation of strong amplitude. Linear flow regime corresponds to smooth movement of free surface and this movement is associated with oscillations of weak amplitude. Duration of these regimes depend upon fill level and deceleration value.

Time period of sloshing in impact regime is different from time period in linear regime which is due to difference in characteristics of activities taking place in both of the regimes. Impact regime is characterized by non-linearity present in the flow. Theoretical sloshing time period can be calculated using following equation:

$$f_s = \frac{1}{2\pi} \left[3.16 + \frac{g}{l} \tanh(3.16 + \frac{h}{l}) \right]^{1/2}$$

Where f_s = sloshing natural frequency,

l= maximum dimension of base of the tank,

h=height of fluid filled in the tank,

g=acceleration due to gravity

Figure 4.36 show the comparison of time period in impact regime and linear regime with theoretical value of time period for different fill levels at deceleration of 0.25g.
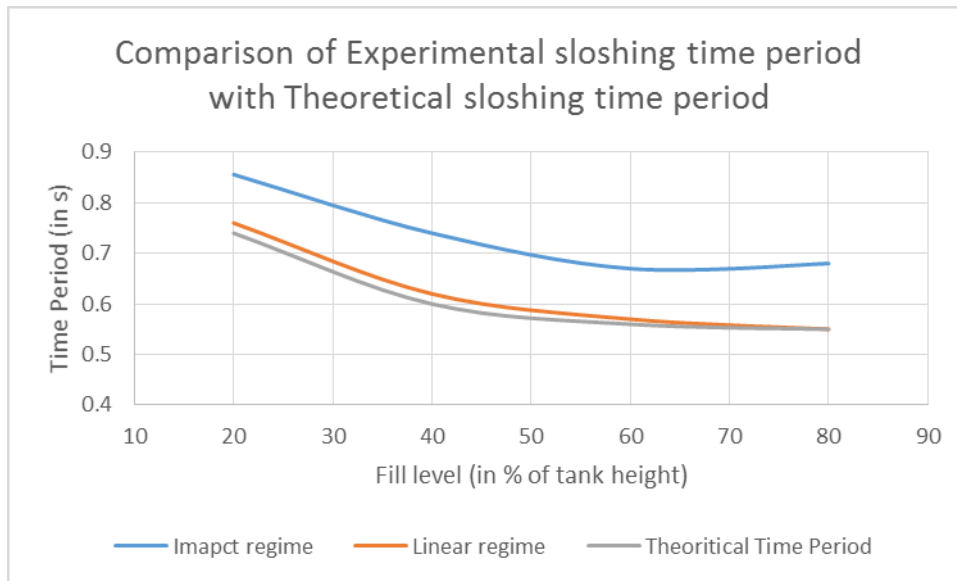
Figure 4.35 Comparison of Experimental time period with Theoretical Time Period

The time period in impact regime is larger than the linear regime for all fill levels. This is due to the fact that in impact regime, sloshing is associated with oscillations of large amplitude and the liquid reaches the tank roof after hit on the wall thus increasing the time period of sloshing. Time period of Sloshing in linear regime is comparable to theoretical time period for all fill levels and exactly matches at 80% of fill level which can be due to large inertial mass associated with this fill level.

Experimental setup developed is able to simulate sloshing and data recorded in different sensors correlates with the high speed camera images. Sloshing phenomenon at different fill levels is observed and is compared for a constant deceleration. At higher deceleration, non-linearity in flow is increased due to the entrapment of air in the flow. At deceleration of 0.3 g, a part of liquid after impact climbs along the wall and get deflected from roof top towards the base of tank and interacts with the wave front travelling in forward direction. This interaction decreases the dynamic pressure at the wall. Sloshing time period in non-linear regime is higher than in linear regime and linear sloshing

time period compares well with theoretical sloshing time period. Transition of sloshing from non-linear to linear is captured in dynamic pressure sensors and high speed camera images and this duration of transition depends on fill level and deceleration value.

Chapter 5: CFD Analysis

5.1 Comparison between 2d and 3d model:

A study was done to check the efficacy of 2d numerical model over 3d model in terms of pressure recorded at certain probe locations. This study was done so as to make further numerical analysis computationally less expensive. The experimental setup developed is designed to simulate sloshing phenomenon due to movement of vehicle in longitudinal direction and the motion in the lateral direction, as discussed in experimental data analysis, was negligible. Ideally the introduction or omission of third direction should not have any significant effects on overall sloshing phenomenon. In order to validate this assumption, 2d and 3d simulations were performed using star ccm+ CFD software with the following specifications.

Fill Level= 20% of tank height

Deceleration value=0.25g

Sensor location=10% of tank height.

A comparison was done with a base mesh size of 3.71875mm (64*64). In order to capture the wall effects, the mesh was made fine near the walls and the near wall mesh size was 40% of base size. Time step used was 0.001s. Comparison was made on the basis of pressure recorded by pressure probes at front and rear walls and the plots are shown in Figure 5.1.

Analysis of pressure plots at front and back boundary shows that both 2D and 3D followed the same trend. However the first peak at the back sensor location is higher in case of 3D simulation while after braking the first peak at front pressure probe location shows higher value for 2D simulation. After the first peak at both the pressure probes, subsequent pressure plots compares well for both the locations.

Computational time for 2D simulation was approximately 2 hours and for 3D simulation was 136 hours, which makes 3d simulation computationally very expensive. Hence all the CFD simulation performed in this study are 2D.
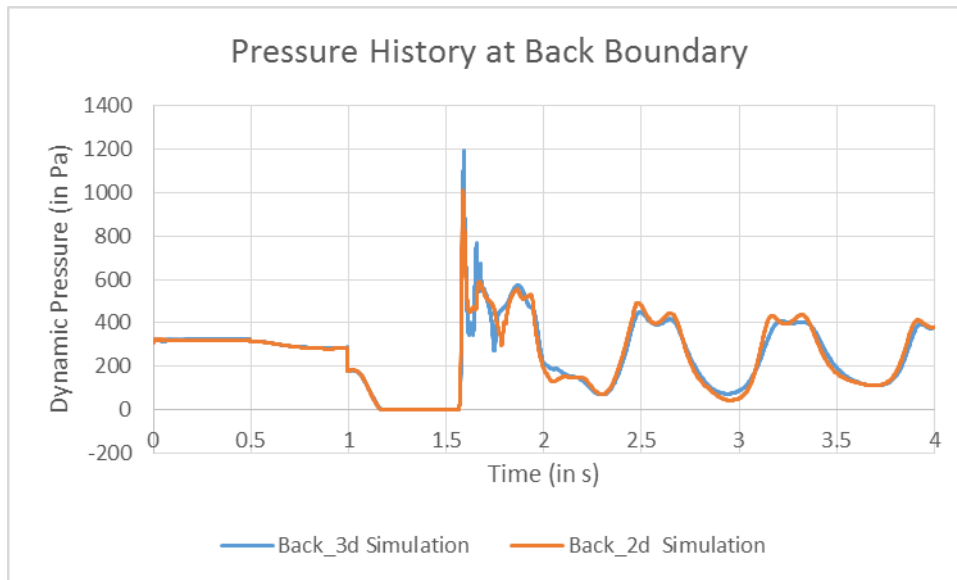
A. Pressure Plot at Back Boundary
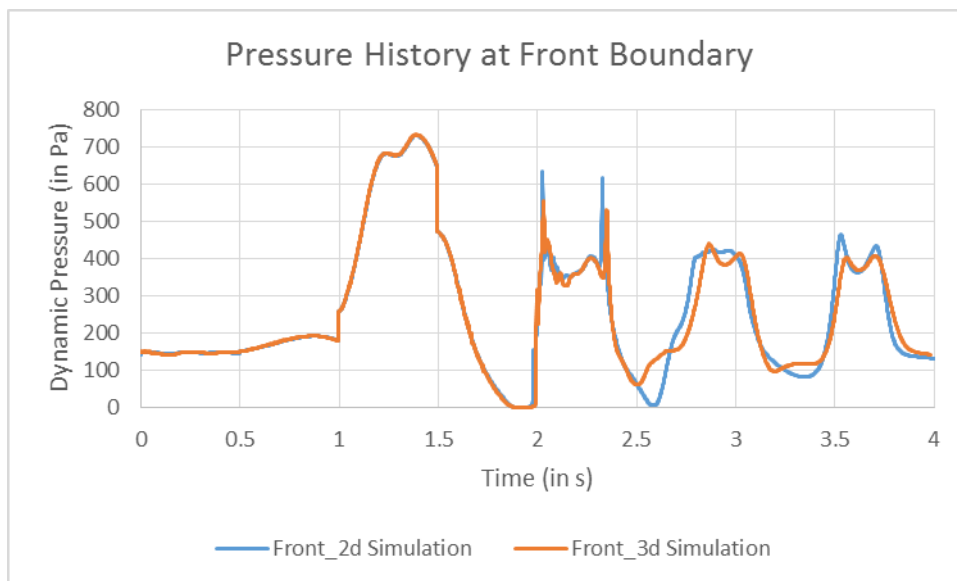
B. Pressure Plot at Front Boundary

Figure 5.1 Comparison between 2D and 3D simulation

5.2 Study for Mesh Independence:

Optimization of mesh size and time step used are essential to make CFD analysis less time consuming and computationally less expensive without loss of important data. Study to see the effects of base size was done in order to select the optimum mesh size. This study was performed on two types of mesh which are:

1.   Uniform Mesh

2.   Fine mesh near the tank walls.

For uniform mesh, study was done for mesh size of 32*32, 64*64 and 128*128 and fill level=20 % of tank height, Deceleration =0.25g and pressure probe location =10 percent of tank height were the specifications of numerical model use for comparison. The pressure plot for back boundary is shown in Figure 5.2. Table 5.1 shows the no. of elements and computational time for all mesh size. The computation time mentioned is the time required to simulate 5s of the flow time.

Table 5.2 Mesh Independence study for uniform Mesh

Mesh-Size	Number of Elements	CPU-Time (in hours)
32*32	1024	10.68
64*64	4096	11.34
128*128	16384	21.56
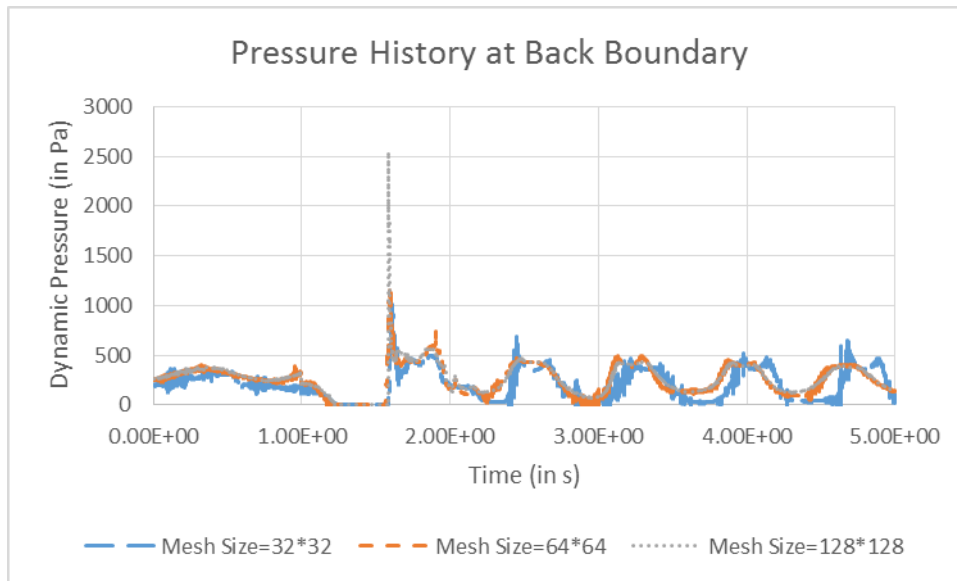
Figure 5.2 Mesh Independence study for uniform mesh

It can be seen from plots shown in Figure 5.2 that the three plots follow similar trend and do not show any significant difference in terms of magnitude except for the first peak. At first peak, the mesh size=64*64 show intermediate value of other two mesh sizes. The 128*128 mesh size show the highest value which may be because the fine mesh is able to resolve the pressure changes near the wall more accurately. However the difference between 64*64 and 128*128 is not significant. Therefore, for future study a mesh size of 64*64 can be used. Fine mesh near the wall will help resolve the near wall flow more accurately. Since the dynamic pressure sensors were mounted with respect to the inner tank walls, a pressure probe that is as close to the wall surface is required. Hence non uniform computational grid was generated. As in the previous study, the base grid size was maintained at 32*32, 64*64 and 128*128. However in this study, the mesh near the walls were refined. The near wall mesh was maintained at 10 % of base size. These cases were setup for a fill level of 20%, deceleration value=0.3g and sensor location of 10% tank height.

Table 4.2.2 shows the number of elements and time taken by all the cases for 20000 time steps.

Table 5.2 mesh Independence study for mesh fine at edges

Mesh-Size	Number of Elements	CPU-Time (in hours)
32*32	13156	8.30
64*64	50117	22
128*128	178203	94

The pressure plot for back boundary is shown in Figure 4.2.3. The time step used for this analysis was 0.0001s. The simulation for mesh size of 128*128 diverged after 2.0s of physical time which might be due to very high value of CFL number at that instant. This is the instant when the fluid after hitting the rear wall is moving towards front wall to make an impact. Similar to the plot for the uniform mesh, in this case also they follow the same trend and do not differ much in terms of amplitude except for the first peak. But the difference in first peak amplitude for three mesh sizes is very small as compared to last case. This is because the mesh is already very fine in all the cases. Since the three mesh sizes do not show any significant difference, the mesh size of 64*64 has been used for further analysis.
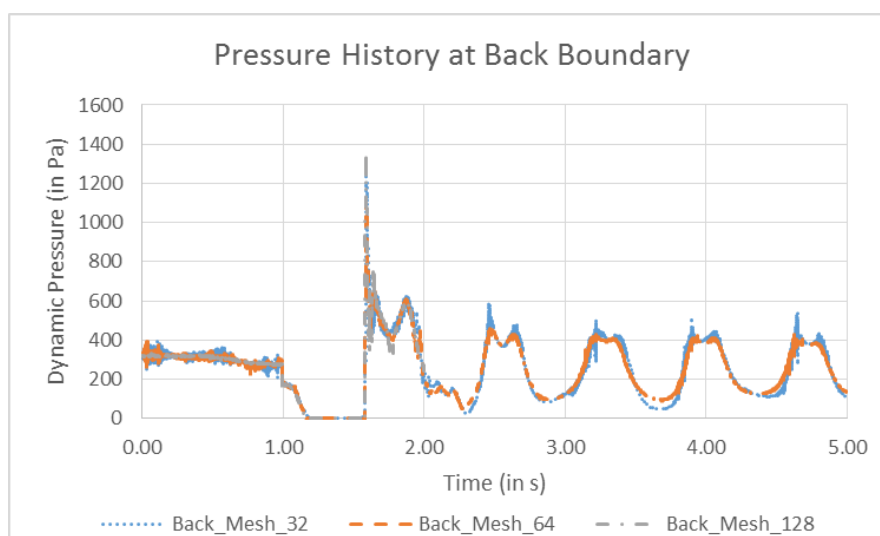

**Figure 5.3 Mesh Independence study for mesh fine at edges.**

5.3 Effect of turbulence:

A case for 20% fill level and a deceleration value of 0.25g was examined to study the effect of turbulence on sloshing phenomenon. The whole simulation was initiated with a velocity of 0.9m/s and the inertial acceleration value was provided from 0.1s before application of brake. The aim of this study was to predict the difference between inviscid, laminar and turbulent simulations. The turbulence models that were taken under consideration were Spalart Allmaras Model, K-Epsilon Model and were compared with laminar and inviscid flow simulations.

The inviscid flow is an idealized situation in which viscous effects are neglected and governing equations are obtained by discarding the viscous term in Navier Stoke's equation and solving these equations would not resolve boundary layer and other viscous effects arising in the flow.

Viscous flows which take viscosity under consideration and can be divided into laminar and turbulent flow and are differentiated on the basis of Reynold's Number. Laminar flows are well ordered flow which do not undergo macroscopic, non-repeating fluctuations. Turbulent flows are the flows that include continuous instability, exhibit irregular, small-scale, highly fluctuating flows in both space and time.

There are a number of models that can simulate these flows but every model is accompanied with certain limitations. The Spalart Allmaras Model solves an equation for turbulent viscosity (ν_t) in terms of $\tilde{\nu}$ where $\tilde{\nu}$ is related to ν_t as $\nu_t = \tilde{\nu} f_v 1$. The k-$\varepsilon$ model solves two equations for k and ε which in turn defines the value of turbulent viscosity (ν_t). This value of turbulent viscosity is used in solving RANS equation.
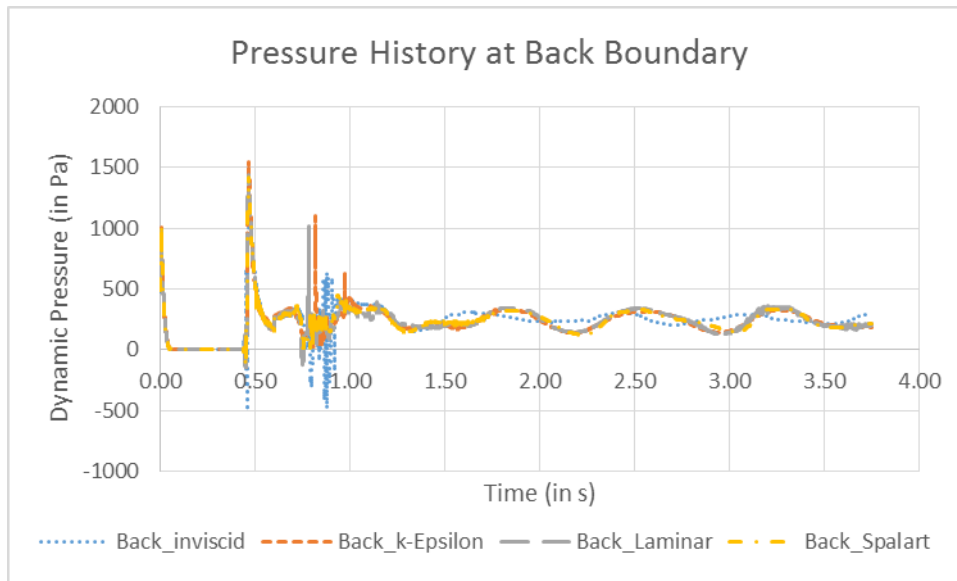
A. Pressure plot for back boundary
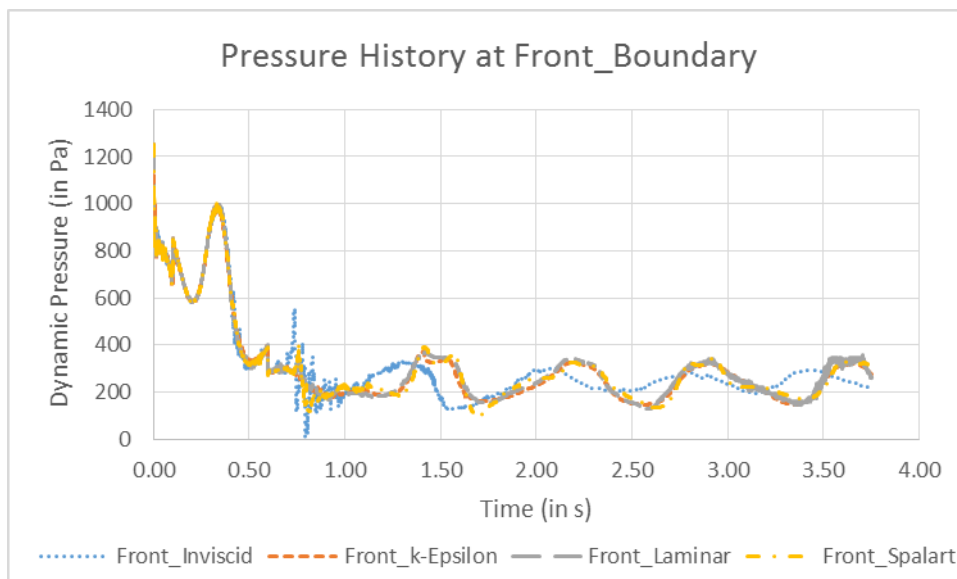
B. Pressure plot for front boundary

Figure 5.4 Comparison of different viscous flow models

Analysis of front and back pressure plots in Figure 5.4 suggested that the inviscid flow model showed some fluctuations in duration of 0.55s to 1s which are not seen in other models plots and it is out of phase when compared to other model plots. Analysis of liquid volume fraction distribution corresponding to inviscid simulation suggested that after impact on rear wall when the fluid was traversing back towards the front wall, a number of local

vortices were generated which were not seen in other simulations which can be attributed to the lack of the viscosity term in inviscid flow. The pressure time history for the laminar and two turbulence models are very close. However as the flow is highly unsteady, turbulent flow modelling is favored as it can resolve the unsteady flow better. As k-ε turbulence model is a more complete model, it was used for all the simulations in this study

The first variable, k determines the turbulence kinetic energy whereas the second variable, ε the dissipation rate of the turbulence kinetic energy. Together they give an estimate of the length and time scale in the turbulent flow.

5.4 Effect of initial conditions:

5.4.1 Comparison between inclined and flat initial interface

Consider a control volume enclosing a certain quantity of fluid and the fluid is at rest with respect to the control volume but the control volume is undergoing constant linear acceleration. The total pressure in such a condition is given by:

$$P = -\rho \left(a_x X + a_y Y + \left(a_z + g \right) Z \right) + P_o \tag{14}$$

Where P=total pressure acting on fluid, ρ= density of fluid, a_x=acceleration in x-direction, a_y=acceleration in y-direction, a_z= acceleration in z-direction, g is gravitational acceleration, X, Y and Z are the coordinates of center of fluid surface and P_o=Atmospheric Pressure. Such a condition for a two dimensional case is shown in Figure 5.5.
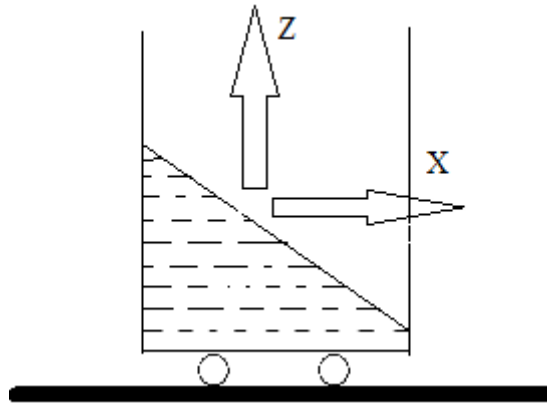
Figure 5.5: Initial Interface due to constant lateral acceleration.

During experiment, the vehicle travelled a distance of 0.65m before DAQ was triggered at a constant acceleration. It can be assumed that at trigger point, fluid has achieved an inclined profile under effect of constant vehicle acceleration. In order to compare the effects of inclined profile on liquid sloshing a case was studied and was compared with simulation in which initialization was done with flat interface.

We have assumed the tank is moving with constant acceleration in x-direction (direction of motion), there is no lateral motion (ay=0) and the gravity acts in z direction. Since the interface is a free surface, so pressure is constant along the surface and is equal to atmospheric pressure. (P=Po).

So the equation modifies to

$$a_xX=-gZ \tag{15}$$

Using this equation, the liquid phase distribution in tank was initialized. This study was done for fill level=20%, deceleration=0.3g and pressure probes were located at 10% of tank height. Figure 5.6 show the initial liquid phase distribution for two simulations and Figure 5.7 shows the comparison between two conditions in terms of dynamic pressure at front and rear wall of tank.
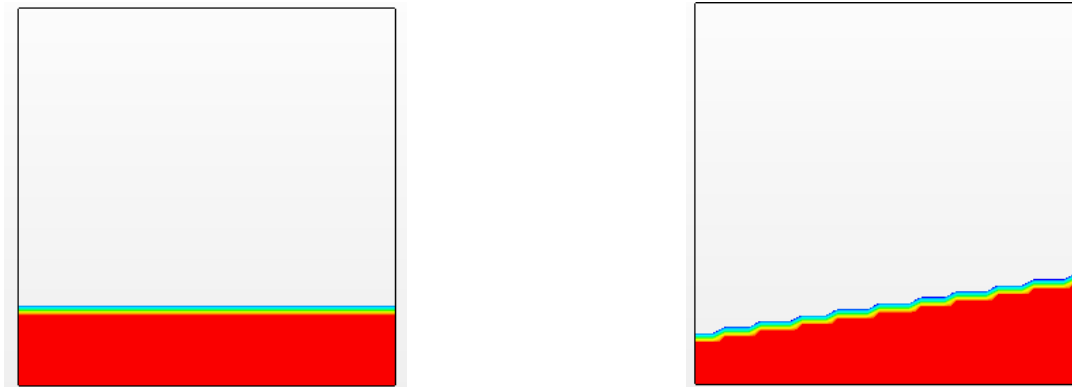
A. Flat Initial condition   **B. Inclined Initial Condition**

Figure 5.6: Initial Liquid phase distribution for two conditions
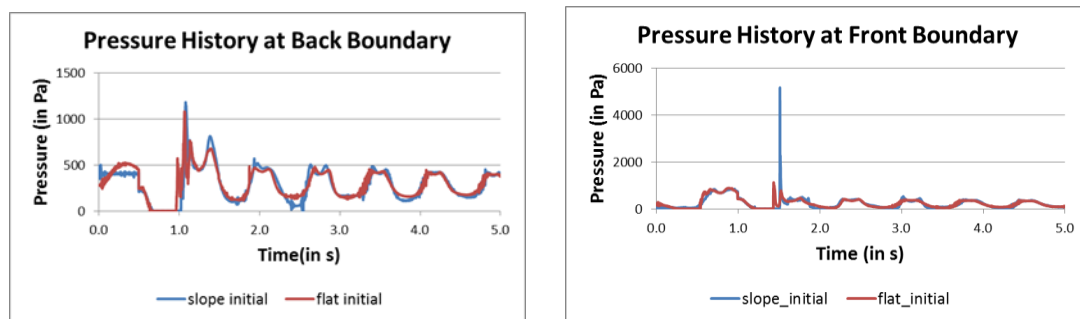
Figure 5.7: Pressure Comparison at back and front boundary for two conditions

It can be observed from plots that pressure plots at back boundary for the two conditions follow similar trend and also there is not much difference in magnitude. Pressure plot at front boundary for inclined initial condition has shown a peak at approximately 1.5s which is larger in magnitude as compared to flat initial condition. But this peak can be due to some localized event taking place in region of pressure probe. Apart from this localized event, pressure history at front boundary is highly close for two initial conditions. Hence a flat interface was used for all the simulations in this study.

5.4.2 Effect of initialization at brake application

Analysis of high speed video images for high deceleration value showed that during braking, fluid moves towards the front wall and almost all fluid got shifted towards the front wall thereby dissipating all the energy and then it

move towards the back wall under the effect of gravity. The instant when the fluid starts moving under the effect of gravity was captured and liquid-air interface tracked from the image was used as initial condition for CFD simulation. This study was done for fill level of 20%, deceleration=0.25g and the pressure probe was kept at 10% of tank height. Figure 5.8 show the high speed video image corresponding to this instant and initial condition derived from this image. Figure 5.9 show the transient acceleration input and dynamic pressure comparison between experiment and simulation for this case.
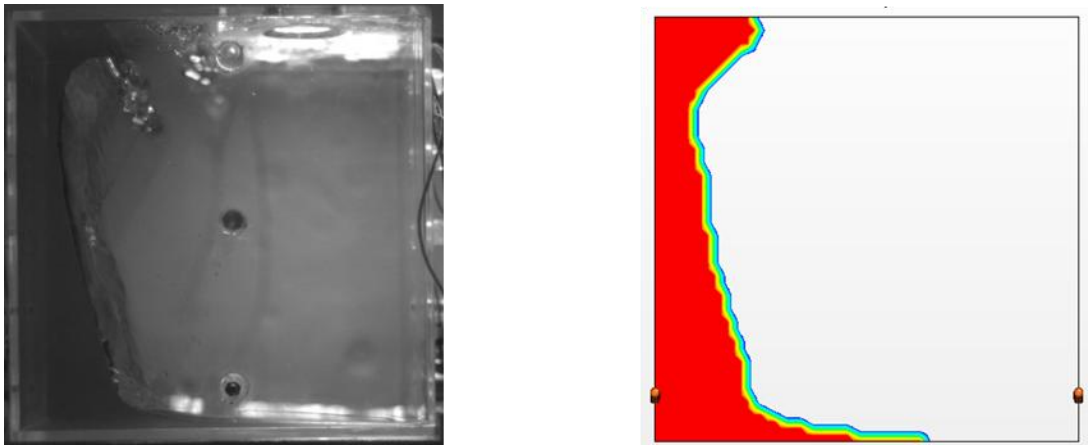
Figure 5.8: High speed camera image and CFD interface corresponding to it
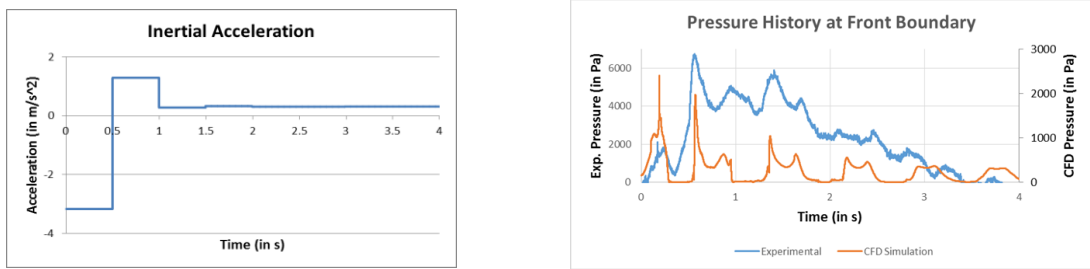
A. Inertial acceleration **B. Pressure History at front Boundary**

Figure 5.9: CFD Input and CFD Pressure comparison with experiment.

It can be observed from the pressure history comparison that CFD is able to predict the trend of the sloshing phenomenon taking place inside the tank. The events although compares well qualitatively but there is much difference

in amplitude of the peaks captured at major events. The CFD simulation is not able to predict the impact flow regime which is associated with presence of entrapped air in the flow. The condition in which almost whole liquid get shifted towards the front wall also occur at high deceleration value and increase in deceleration value raises the non-linearity in flow.

5.4.3 Effect of initialization before first impact event

High speed camera images before first impact at back wall were analyzed and it was observed that a wave front was travelling towards the front wall. A number of successive images were captured and distance travelled by the wave front in successive images was recorded and using the distance travelled and time frame of these images velocity of wave front was determined. This velocity along with the liquid-air interface was used to initialize the CFD simulation.

Figure 5.10 show the successive images used for calculating velocity of wave front. Figure 5.11 show the initial liquid phase distribution tracked from high speed camera image and initial velocity field used for this simulation. Figure 5.12 refers to the inertial acceleration used as input and pressure comparison between experiment and CFD

| t=1.2748 s | t=1.2828s | t=1.3788s |
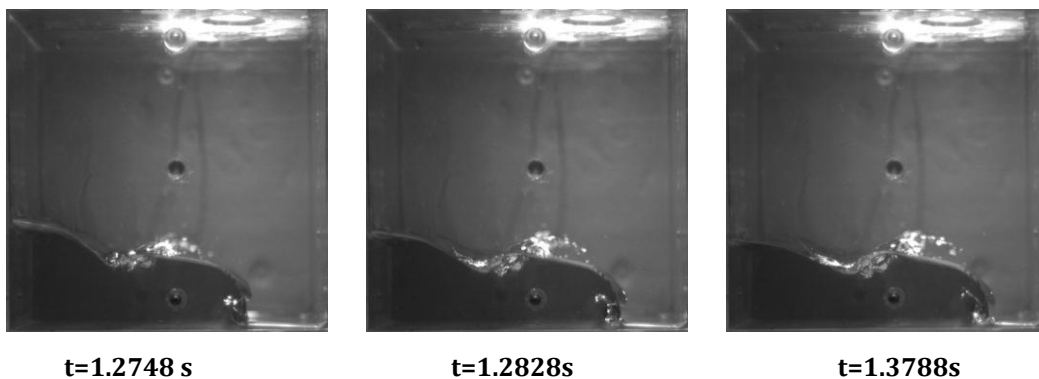
Figure 5.10: High speed Camera images used for velocity calculation
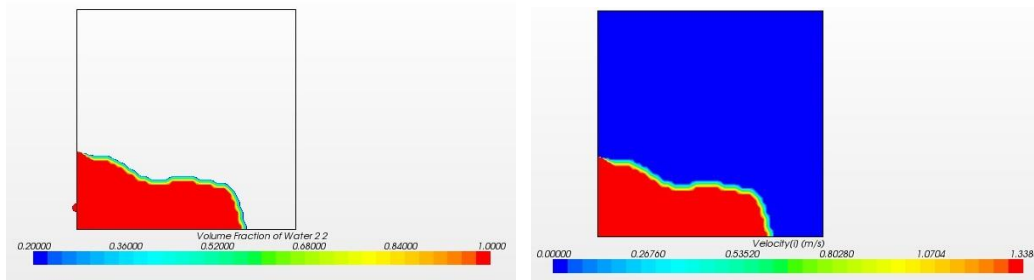
Figure 5.11: Initial Liquid phase distribution and velocity field used in CFD
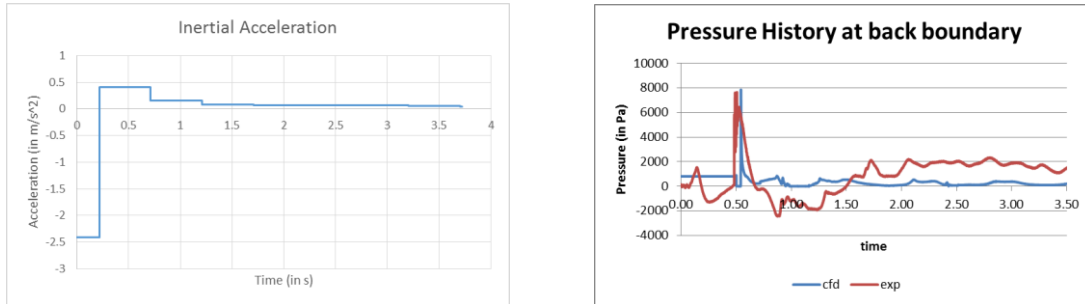
Figure 5.12: Inertial acceleration input and pressure comparison at back boundary

It can be observed from the dynamic pressure comparison between experiment and CFD that this approach is able to predict the pressure at back wall during first impact however after this event it underestimates the pressure for upcoming events at back wall as can be observed from the plot. After first event CFD is able to predict the trend but there is much difference between CFD and experimental pressure in magnitude.

The two approach discussed in last two subsections are not practical as these approach need liquid phase distribution from the experiment. The first approach is not able to predict the major events in terms of magnitude while the second approach can only predict the first event and cannot simulate the upcoming events quantitatively. There was not much difference in results of simulation when one was initialized with a flat free surface while the other was initialized with an inclined free surface. Hence a flat surface with no velocity initialization was used for CFD analysis.

91

5.5 Liquid Phase Distribution Comparison between CFD and Experiment:

In order to validate the CFD model, liquid phase distribution captured for simulation were compared with high speed camera images recorded during experimentation. The CFD simulation were carried out using inertial acceleration data recorded during the experimental study. This study has been carried out for two fill levels of 20 % and 60 % and a constant deceleration value of 0.25g. The comparison has been made for two different time steps in each case.

To quantify the comparison between the CFD and experimental results, the difference between the liquid surface height obtained from CFD and experiment is compared and tabulated in tables attached besides the comparison. Several points were defined on the liquid surface and the ratio of interface height to distance from front wall is tabulated. This comparison is performed in the near linear sloshing regime because in the non-linear sloshing regime, there is large entrapment of bubbles which make the image interrogation for liquid surface very difficult. It must also be noted that the image interrogation technique presented here has a few sources of uncertainty which are:

1. Liquid surface determination for bubbly flow is difficult to measure

2. Liquid surface height is again difficult measure when the liquid height is small because meniscus effect due to wall wetting leads to uncertainty   of surface location.

3. Perspective projection of a 3D image on a 2D surface leads to parallax effects which may again lead to uncertainty in image interrogation.

These uncertainties are higher in non-linear flow regime and subsequently decrease in the linear slosh regime. Hence the measurements presented in the two tables are at time instances when the flow is in the linear flow regime.

In Figure 4.2.5, the liquid volume fraction is compared with the corresponding experimental for fill level of 20 percent and deceleration value of 0.25g. The first image refers to the time of application of the brake. At this instance, the liquid surges towards the fr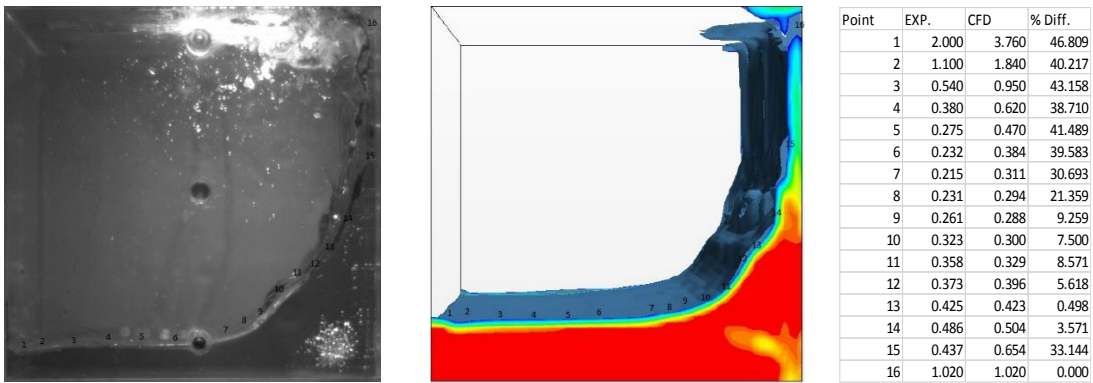ont end of the wall. The CFD and experimental results compare well qualitatively. However quantitative comparison at few discrete locations reveal that there is some difference in the liquid heights that is predicted from CFD simulation when compared with liquid height that is obtained from high speed video images. The percentage difference in liquid height is more apparent for lower liquid height than for regions where the overall liquid height is large. This is because of the lower base value while calculating the percentage error for regions where the liquid height is low. The second set of images in Figure 5.13 is when the liquid sloshes back towards the rear wall. Here the slosh magnitude is higher than the first instance and liquid reaches the roof of the tank. A bubble entrapped near the bottom of the rear wall can be seen in both CFD as well as Experimental results. CFD again broadly captures this state of the liquid in the tank.
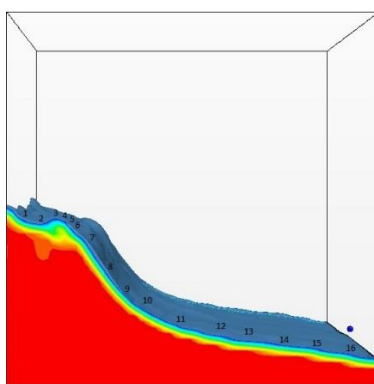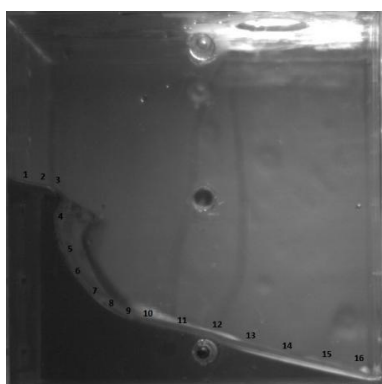
Point	Exp.	CFD	% Diff.
1	11.960	9.880	17.391
2	5.840	4.720	19.178
3	3.813	3.373	11.538
4	3.125	3.063	2.000
5	2.167	2.589	19.487
6	1.640	2.270	38.415
7	1.056	1.648	56.061
8	0.727	1.147	57.798
9	0.577	0.611	5.941
10	0.500	0.540	8.000
11	0.364	0.360	1.099
12	0.253	0.257	1.316
13	0.171	0.197	15.000
14	0.118	0.158	34.043
15	0.076	0.116	52.941
16	0.032	0.096	200.000

Fill Level=20% of tank height, Time=1.3s

Point	EXP.	CFD	% Diff.
1	2.000	3.760	46.809
2	1.100	1.840	40.217
3	0.540	0.950	43.158
4	0.380	0.620	38.710
5	0.275	0.470	41.489
6	0.232	0.384	39.583
7	0.215	0.311	30.693
8	0.231	0.294	21.359
9	0.261	0.288	9.259
10	0.323	0.300	7.500
11	0.358	0.329	8.571
12	0.373	0.396	5.618
13	0.425	0.423	0.498
14	0.486	0.504	3.571
15	0.437	0.654	33.144
16	1.020	1.020	0.000

Fill Level=20% of tank height, Time=1.75s

Figure 5.13 Phase Field Validation for Fill Level =20 %

The second comparison has been done for 60 percent of fill level and is shown in Figure 5.14. When compared with Figure 5.5, the sloshing magnitude for 60% fill level is less compared to the sloshing magnitude for 20% fill level. This is because, due to increased mass, the liquid has to overcome the larger initial inertia, which is contributing to lower magnitude. However, when the liquid retraces to the rear of the tank, there is large air entrainment and the liquid surface becomes very bubbly. The surface profile from CFD is comparable to the images from high speed video.

Point	EXP.	CFD	% Diff.
1	0.931	0.912	2.062
2	0.902	0.871	3.398
3	0.820	0.836	1.887
4	0.790	0.819	3.586
5	0.724	0.789	9.014
6	0.664	0.729	9.753
7	0.622	0.673	8.266
8	0.609	0.611	0.441
9	0.568	0.572	0.748
10	0.512	0.521	1.843
11	0.458	0.480	4.827
12	0.410	0.479	16.703
13	0.351	0.490	39.661

Fill Level= 60% of tank height, Time =0.7s

94

Point	EXP	CFD	% Diff.
1	0.468	0.528	12.975
2	0.494	0.466	5.540
3	0.506	0.477	5.735
4	0.503	0.494	1.675
5	0.547	0.538	1.775
6	0.527	0.590	12.018
7	0.627	0.622	0.782
8	0.720	0.684	4.951
9	0.911	0.726	20.351
10	0.917	0.735	19.809
11	0.926	0.784	15.333

Fill Level=60% of tank height, Time= 3.0s

**Figure 5.14 Phase Field Validation for Fill Level =60 %**

For 60% fill, the percentage error is smaller. The CFD simulation does capture the size of the liquid along the wall and finally hitting the tank roof. The % error near the front wall is relatively large. This indicates that larger amount of liquid remains along the bottom surface of the tank and less amount of liquid has climbed vertically along the back wall.

5.6 Dynamic Pressure Comparison between CFD and Experiment:

The dynamic pressure sensor used in the experiments consist of quartz discs attached to a diaphragm. Pressure acting on the diaphragm compresses the quartz discs and produce electrical charge which is converted to pressure acting on the sensor using sensitivity of the respective sensor. The Pressure obtained from CFD is the Pressure field obtained when all the equations of CFD model are converged.

Pressure between CFD and experiment was compared for following cases:

1.   Fill level=40 %, Deceleration=0.25g

2.   Fill level=60 %, Deceleration=0.25g

3.   Fill level=80 %, Deceleration=0.25g
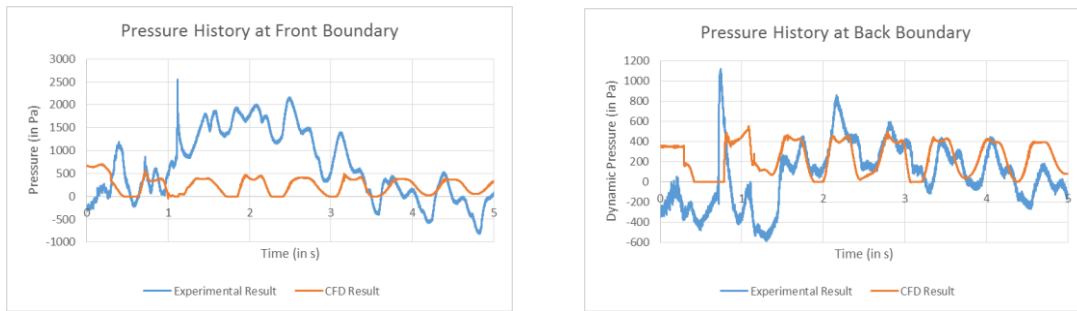
A. Fill level=40%, Deceleration=0.25g, Pressure Probe=30% of tank height
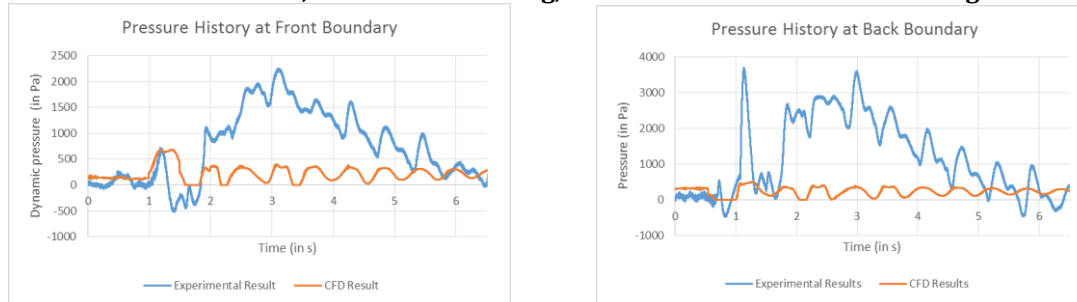
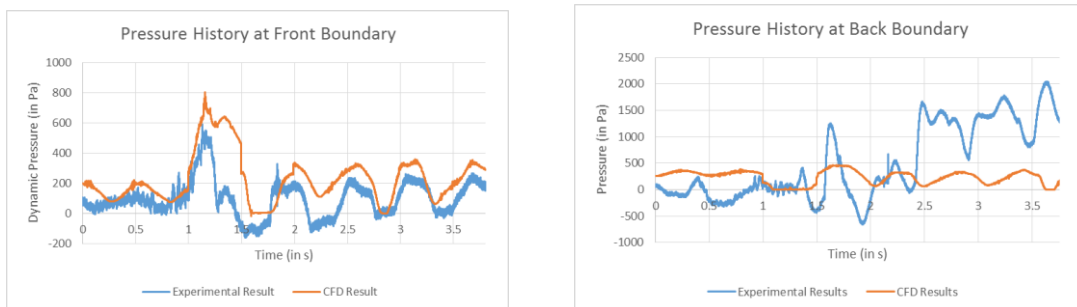**B. Fill level=60%, Deceleration=0.25g, Pressure Probe=50% of tank height**

C. Fill level=80%, Deceleration=0.25g, Pressure Probe=70% of tank height

Figure 5.15 Dynamic Pressure Comparison for various cases.

Figure 5.15 A, B and C represents the comparison of dynamic pressure between CFD and experiment for 40%, 60% and 80% case. All these comparisons are made for deceleration value of 0.25g and pressure probes were placed at a location of 10 percent below fill level.

Pressure Plots shown in Figure A comprises comparison for 40 percent of fill level. The pressure comparison is done for pressure at back boundary and front boundary. Experimental dynamic pressure plot at back boundary shows that

the transition flow regime between impact flow and linear regime is of very small duration. The CFD pressure plots follow the trends as recorded in experimental data, however they differ in amplitude for the first two peaks. This can be due to non-linearity associated with this flow. But after two peaks since the flow is moving towards linear regime, CFD plots follow the experimental pressure data in terms of trend as well as in terms of magnitude. CFD pressure plot at front boundary follow the same trend as observed in experimental data although the plots differ in magnitude which is due to the non-linearity associated with the flow.

Figure B refers to the comparison made for 60 percent of fill level. The comparison is made for Pressure at front boundary. Analysis of experimental pressure data suggested that the phenomenon for this flow is associated with an impact flow regime and a significant transition zone. The first peak in the plot at 1.2 s refers to the condition when the fluid is moving along the front wall smoothly due to application of brake. This event is linear and hence is recorded in both CFD and experiment with the same order of pressure magnitude. However after this the flow enters the no linear regime where CFD is not able to capture the pressure peaks of same magnitude as recorded in experiment. At 6s when the flow is moving towards the linear zone the CFD has captured the peak of same magnitude and of same trend as recorded in experiments. CFD pressure plot at back boundary follow the same trend as observed in experimental data although the plots differ in magnitude which is due to the non-linearity associated with the flow.

Figure C corresponds to pressure comparison for 80 percent of fill level. The comparison is done for front boundary and the sensor is mounted at 70 percent of tank height. The sloshing phenomenon for this fill level is liner due to large

mass of fluid associated with this fill level. The CFD and Experimental Pressure plots follow the same trend as well as are of same order. Pressure plots at back boundary for this fill level shows that CFD is not able to capture the sloshing phenomenon in terms of magnitude but the major events are observed at same time in both the experimental and CFD pressure plot.

It can be concluded that CFD can predict the flow trend and can capture the pressure trends at respective boundary. When the flow is linear and smooth, the pressure captured in CFD simulation compares well with experimental pressure, but when the flow is associated with non-linearity, the comparison can only be made qualitatively as the plots differ in magnitude. This difference can be due to bubbles entrapped in transition flow.

The impact pressure regime can be calculated if initial velocity field and initial phase field used in simulations are similar to experimental conditions at the time of sensor trigger.

Chapter 6: Conclusion and Future Work

Experimental setup developed for study of sloshing phenomenon is able to capture all the major events taking place inside the tank. The events captured in the dynamic quantity sensors were supported well by high speed camera images at that instant. The dynamic force sensor peaks were in trend with the events recorded in dynamic pressure sensor. Dynamic pressure sensor at front wall has shown a trough when a crest is recorded in the pressure sensor at rear wall which was as expected. Three distinct flow regimes viz. impact regime, transition regime and linear regime were observed in dynamic pressure sensor data.

CFD study in order to check the efficacy of 2d simulation over 3d simulation was done and 2d model was found suitable for further CFD analysis. Mesh independence study was done on uniform mesh as well as on mesh fine at edges and mesh size of 64*64 was used for further analysis. A study was done to evaluate different turbulence models and to compare the results with laminar and inviscid flow and standard k-ε model was opted for numerical analysis.

Images from high speed video camera and dynamic pressure measurement data have been used to compare with developed numerical model. Liquid volume fraction distribution captured during numerical simulation compare well with high speed camera images when the flow is in the linear flow regime. Numerically estimated pressure matches with experimental pressure data well in the linear sloshing regime .CFD simulation performance was much poorer in the non-linear sloshing regime. It could predict well sloshing frequency. However there was large difference in the pressure data when compared with the experimental study.

Future Work

i. Numerical Methodology to predict sloshing in non-linear regime has to be developed. This includes prediction of initial velocity profile and initial fluid-air interface in tank at the time of trigger that can be done using Particle image velocimetry technique.

ii. Study of sloshing in tanks with different aspect ratios and in actual automotive fuel tank needs to be performed.

iii. Development of an analytical model which compares well with numerical and experimental methodology.

iv. Sloshing phenomenon in a reciprocating test setup need to be studied to have in depth understanding of different physics involved in this phenomenon.

v. PIV study needs to be done to predict initial velocity field for numerical simulations.

References

[1]   C. Wachowski, J. W. Biermann, and R. Schala, "Approaches to analyse and predict slosh noise of vehicle fuel tanks."

[2]   L. Khezzar, A. Seibi, and A. Goharzadeh, "Water Sloshing in Rectangular Tanks–An Experimental Investigation & Numerical Simulation," *Int J Ingineering IJE*, vol. 3, no. 2, pp. 174–184, 2009.

[3]   H. Rezaei and M. J. Ketabdari, "Numerical Modelling of Sloshing with VOF Method," 2007.

[4]   M. Hinatsu, Y. Tsukada, R. Fukasava, and Y. Tanaka, "Experiments of two-phase flows for the joint research," in *Proc. SRI-TUHH mini-Workshop on Numerical Simulation of Two-Phase Flows, Ship Research Institute, Tokyo*, 2001.

[5]   S. aus der Wiesche, "Noise due to sloshing within automotive fuel tanks," *Forsch. Im Ingenieurwesen*, vol. 70, no. 1, pp. 13–24, Feb. 2005.

[6]   O. R. Jaiswal, S. Kulkarni, and P. Pathak, "A study on sloshing frequencies of fluid-tank system," in *Proceedings of the 14th World Conference on Earthquake Engineering*, 2008, pp. 12–17.

[7]   M. Perić and T. Zorn, "Simulation of Sloshing Loads on Moving Tanks," 2005.

[8]   K. P. Thiagarajan, D. Rakshit, and N. Repalle, "The air–water sloshing problem: Fundamental analysis and parametric studies on excitation and fill levels," *Ocean Eng.*, vol. 38, no. 2, pp. 498–508, 2011.

[9]   L. Hou, F. Li, and C. Wu, "A numerical study of liquid sloshing in a two-dimensional tank under external excitations," *J. Mar. Sci. Appl.*, vol. 11, no. 3, pp. 305–310, 2012.

[10] M. Hattori, A. Arami, and T. Yui, "Wave impact pressure on vertical walls under breaking waves of various types," *Coast. Eng.*, vol. 22, no. 1, pp. 79–114, 1994.

[11] C. Lugni, M. Brocchini, and O. M. Faltinsen, "Wave impact loads: The role of the flip-through," *Phys. Fluids 1994-Present*, vol. 18, no. 12, p. 122101, 2006.

[12] L. Di Matteo, F. Fortunato, P. Oliva, and N. Fiore, "Sloshing Analysis of an Automotive Fuel Tank," 2006.

[13] T. M. Wasfy, J. O'Kins, and S. Smith, "Experimental validation of a time-accurate finite element model for coupled multibody dynamics and liquid sloshing," DTIC Document, 2007.

[14] J.-S. Park, S.-C. Choi, and S.-G. Hong, "The prediction of fuel sloshing noise based on fluid-structure interaction analysis," *SAE Int. J. Passeng. Cars-Mech. Syst.*, vol. 4, no. 2, pp. 1304–1310, 2011.

[15] V. V. S. Vytla and Y. Ando, "Fluid Structure Interaction Simulation of Fuel Tank Sloshing," *Optimization*, vol. 2013, pp. 01–09.

[16] U. CD-adapco, *GUIDE: STAR-CCM+*. Version, 2009.

[17] M. Perić and T. Zorn, "Simulation of sloshing loads on moving tanks," in *ASME 2005 24th International Conference on Offshore Mechanics and Arctic Engineering*, 2005, pp. 1017–1026.